Electronic Supplementary Information

Rational design and synthesis of Y-shaped fluorophores with multifarious emission properties and their application in sensitive detection of PA

Si-Hong Chen[a], Kai Jiang[c,]*, Jian-Yun Lin[a], Kai Yang[a], Xi-Ying Cao[a], Xiao-Yan Luo[a], Zhao-Yang Wang[a,b,]*

[a] *School of Chemistry, South China Normal University; Key Laboratory of Theoretical Chemistry of Environment, Ministry of Education; Guangzhou Key Laboratory of Analytical Chemistry for Biomedicine, Guangzhou 510006, China*

[b] *Key Laboratory of Functional Molecular Engineering of Guangdong Province, South China University of Technology, 381 Wushan Road, Guangzhou 510640, China*

[c] *Key Laboratory of Functional Molecular Engineering of Guangdong Province, School of Chemistry and Chemical Engineering, South China University of Technology, Guangzhou 510640, China*

E-mail: wangzy@scnu.edu.cn; Fax: (+86) 20-39310187; Tel.: (+86) 20-39310258

E-mail: 201910104301@mail.scut.edu.cn.

Contents

1. Characterization spectra of synthesized compounds

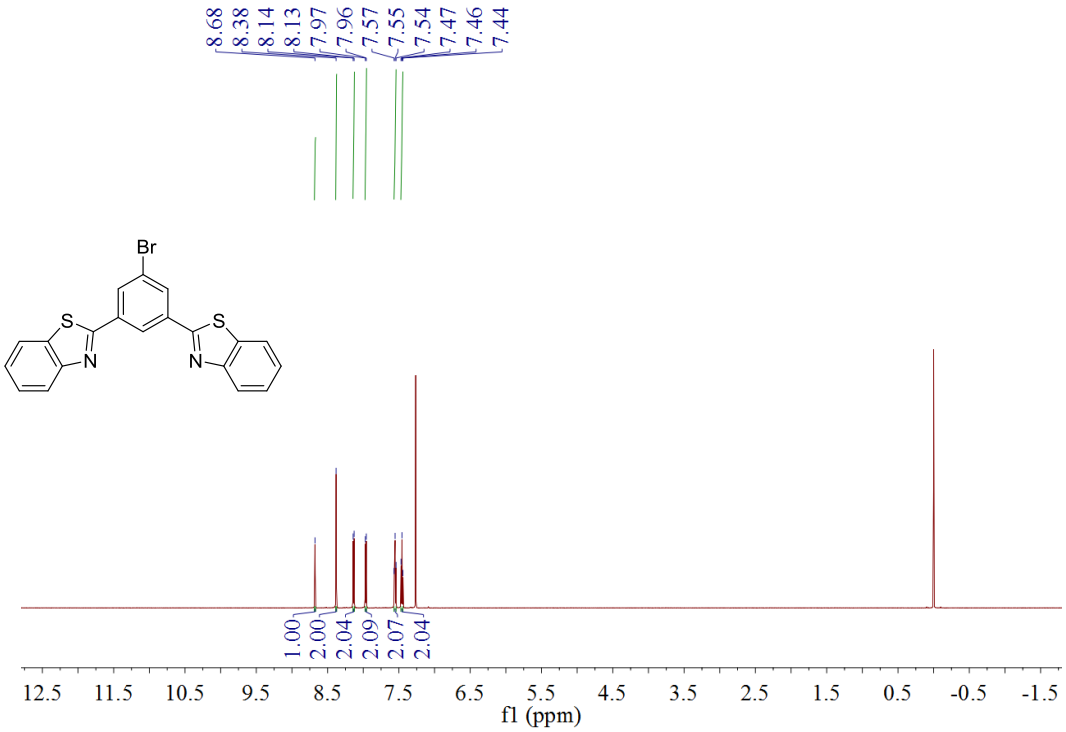

Fig. S1. ^{1}H NMR spectrum of compound **2**.

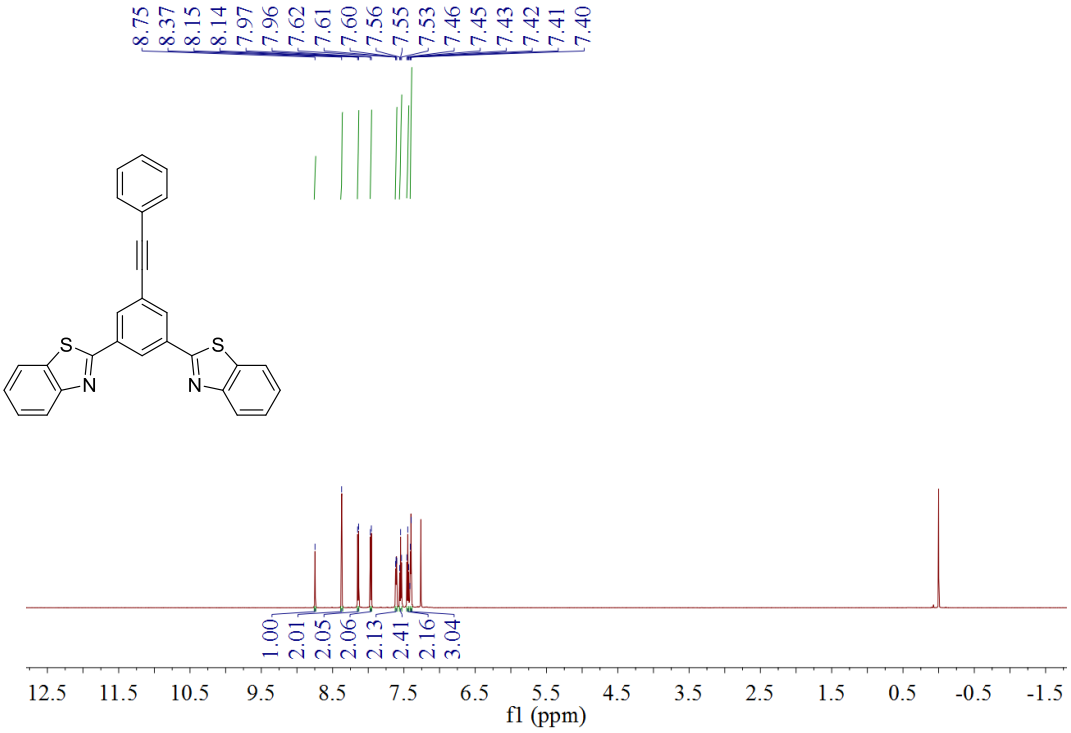

Fig. S2. ^{1}H NMR spectrum of compound **3a**.

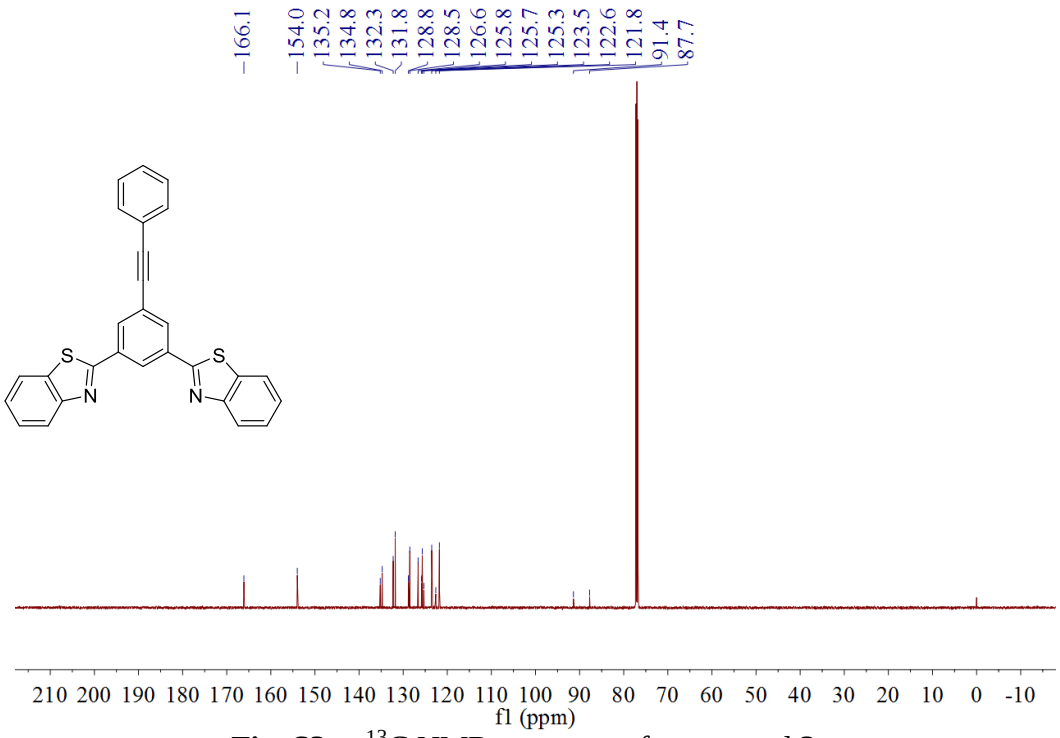

Fig. S3. ^{13}C NMR spectrum of compound **3a**.

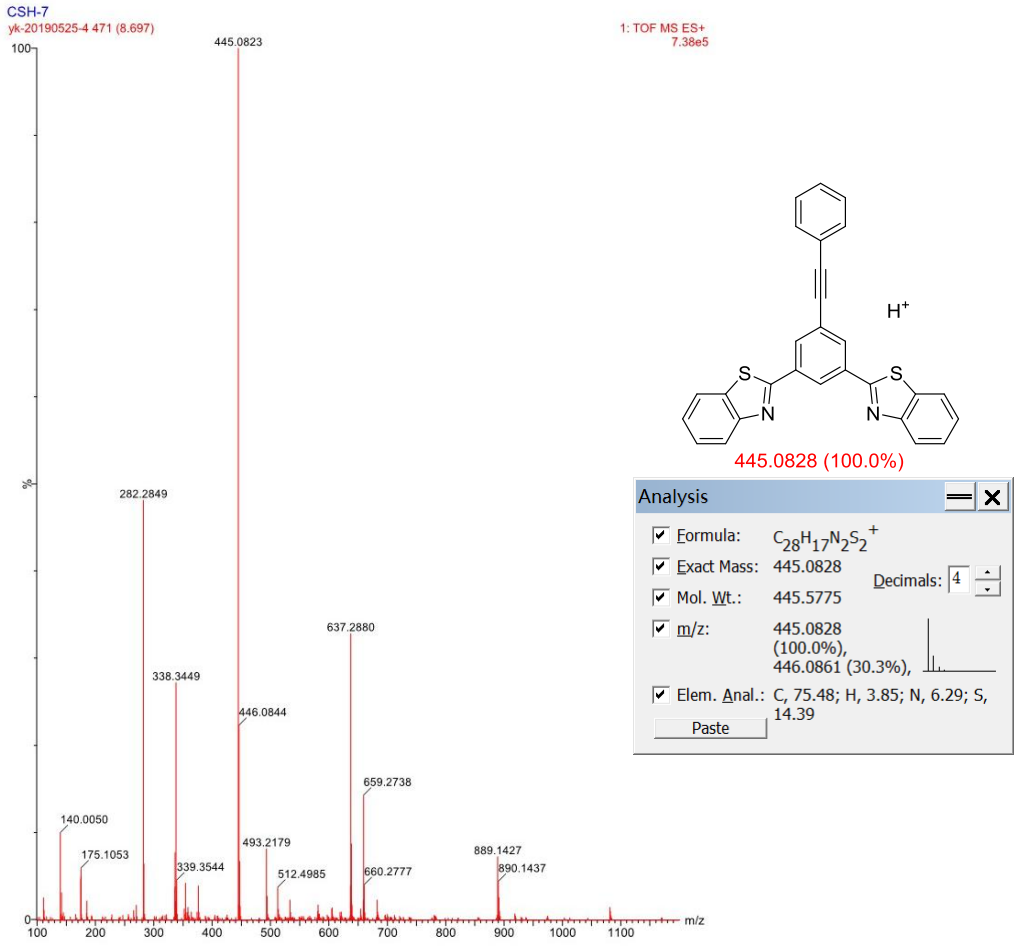

Fig. S4. HRMS spectrum of compound **3a**.

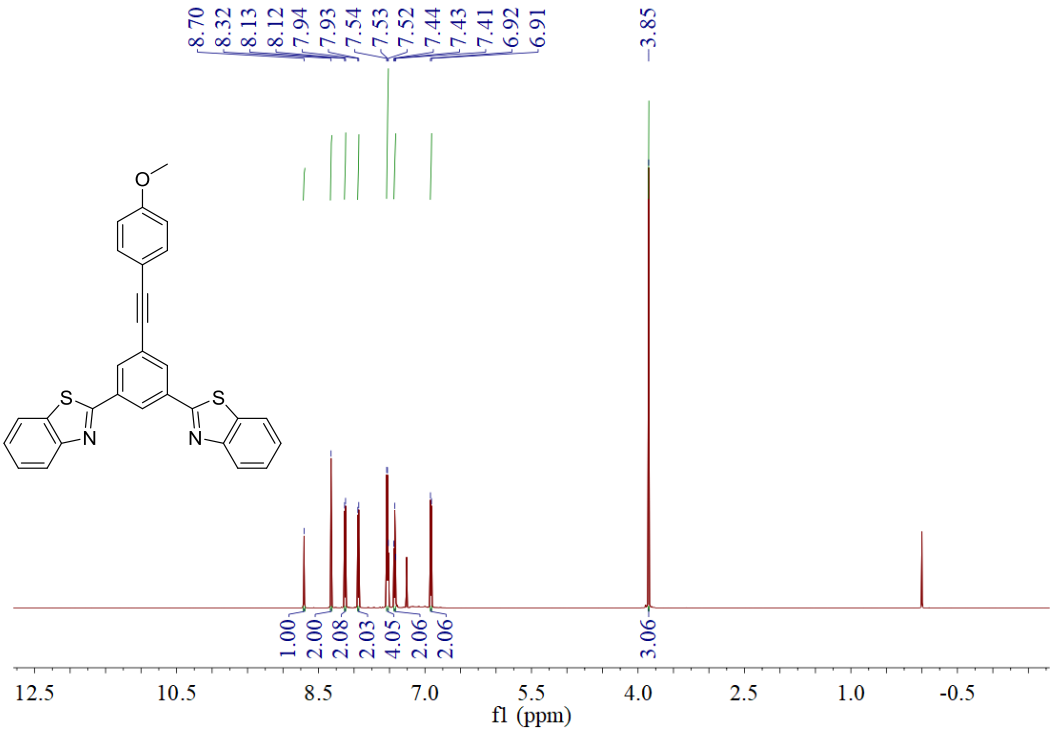

Fig. S5. ^{1}H NMR spectrum of compound **3b**.

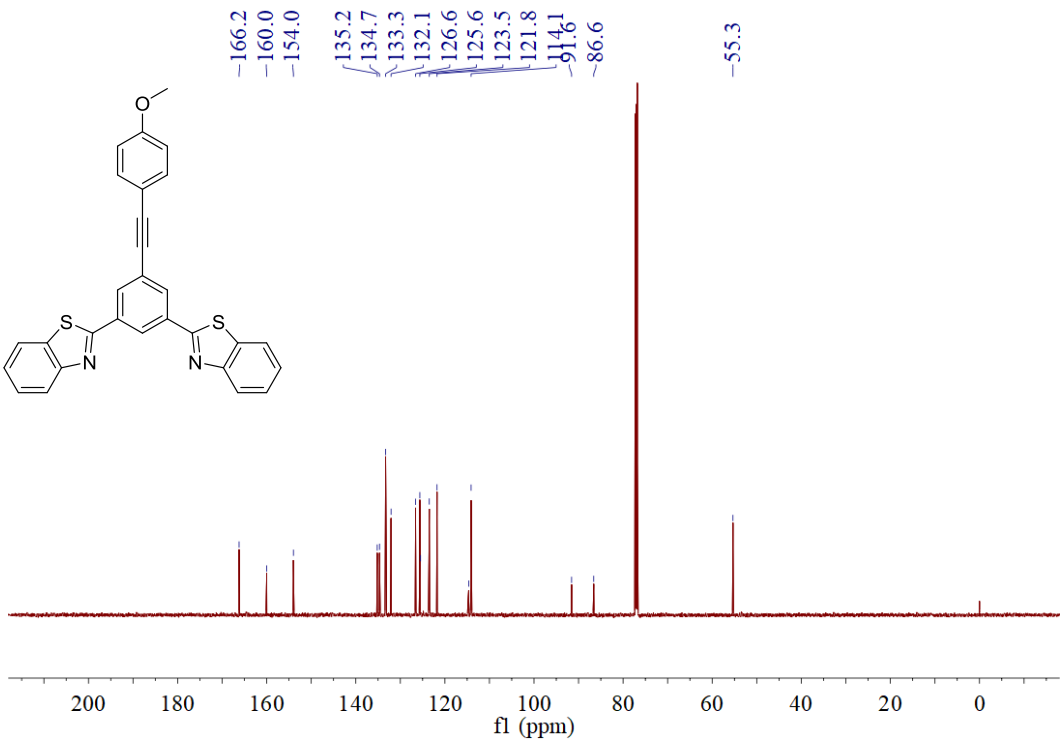

Fig. S6. ^{13}C NMR spectrum of compound **3b**.

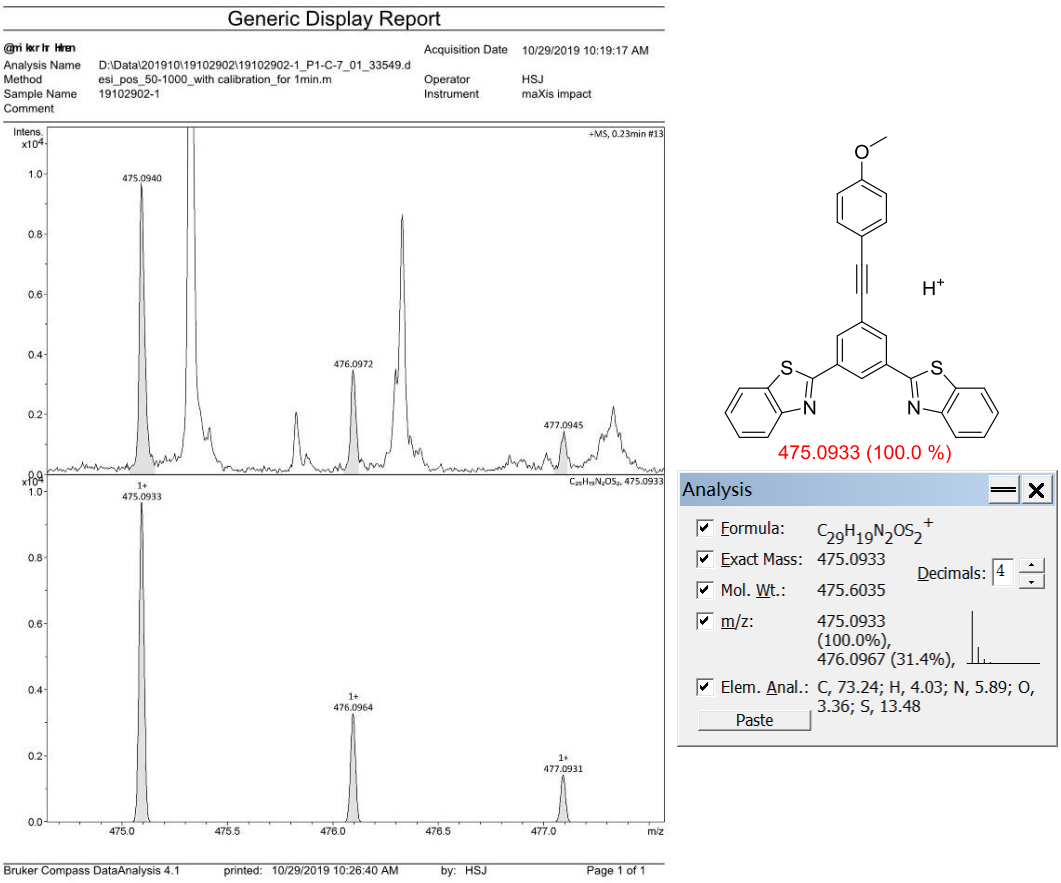

Fig. S7. HRMS spectrum of compound **3b**.

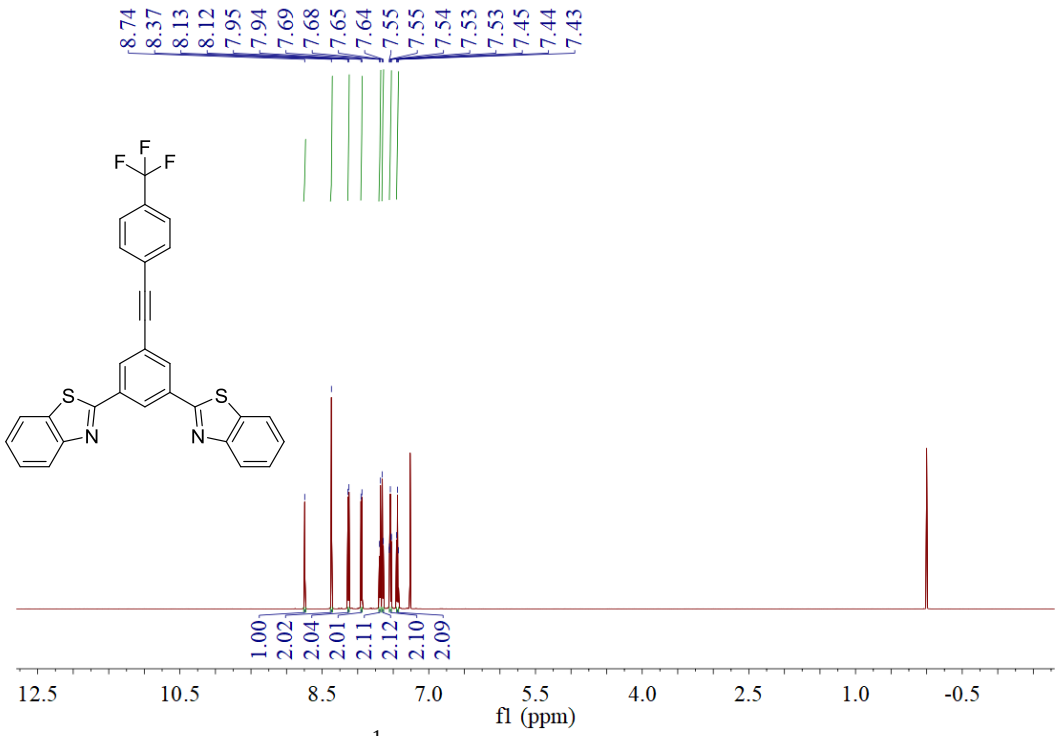

Fig. S8. ^{1}H NMR spectrum of compound **3c**.

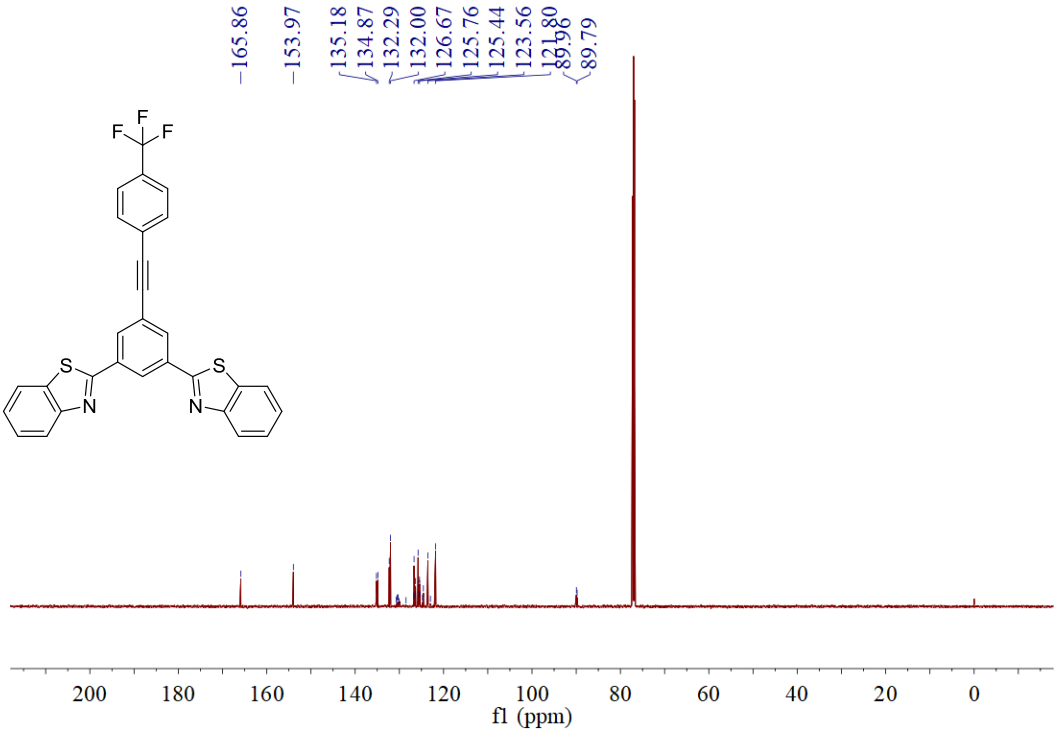

Fig. S9. ^{13}C NMR spectrum of compound **3c**.

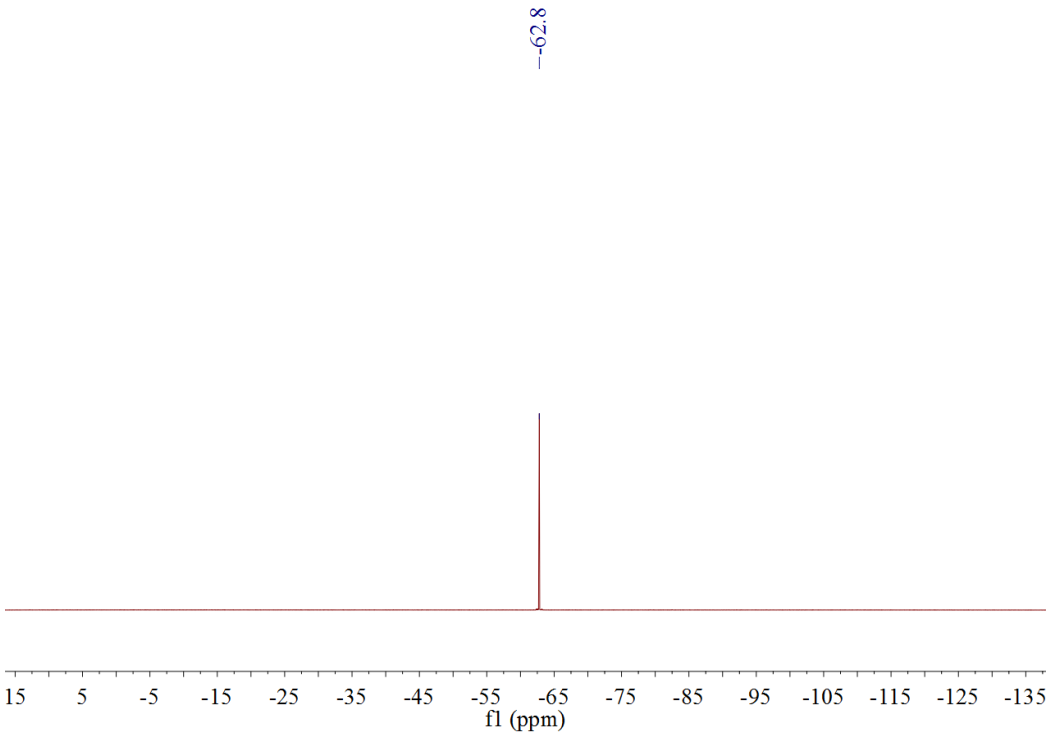

Fig. S10. ^{19}F NMR spectrum of compound **3c**.

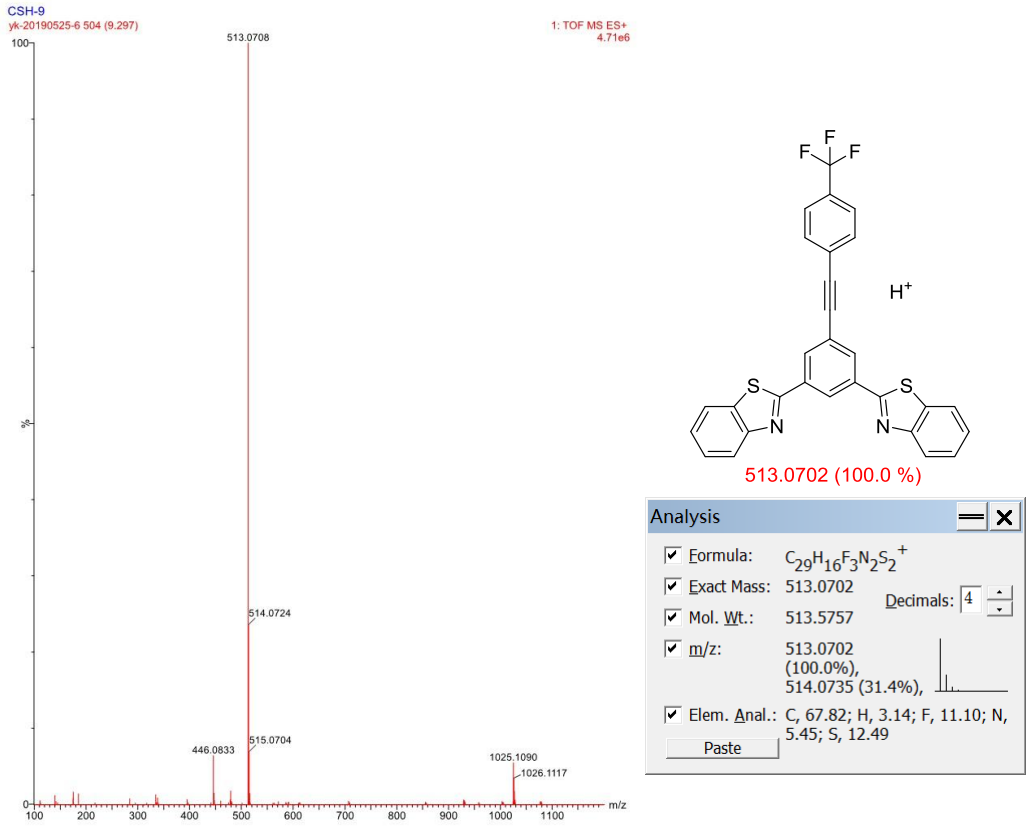

Fig. S11. HRMS spectrum of compound **3c**.

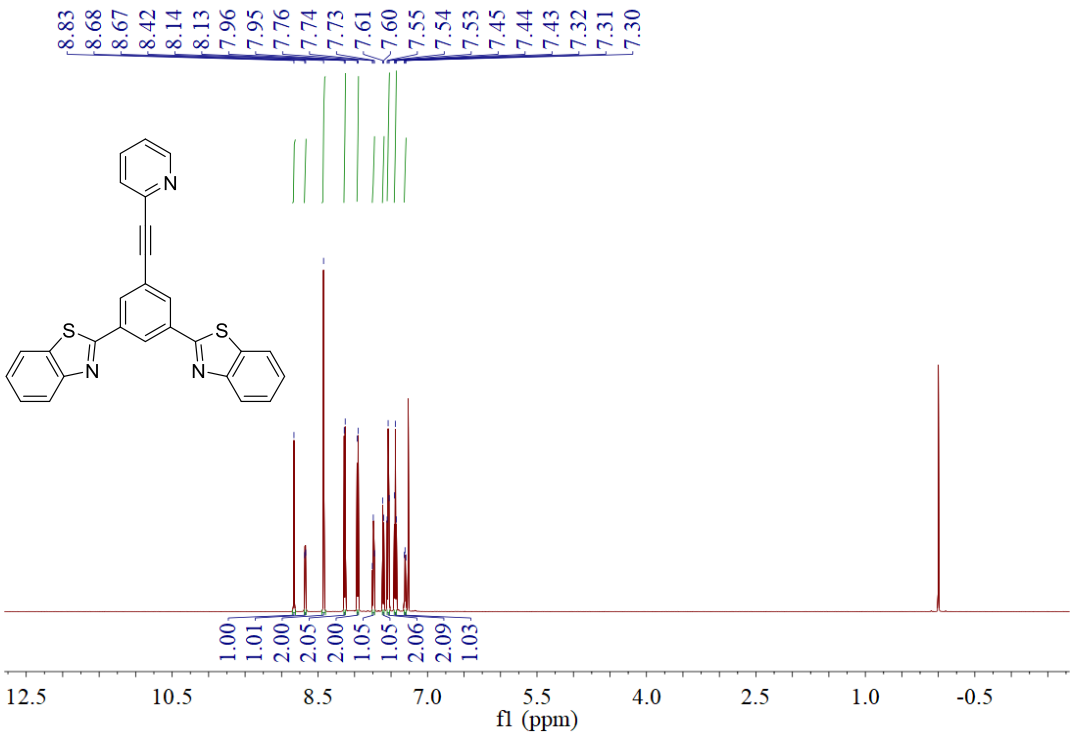

Fig. S12. ^{1}H NMR spectrum of compound **3d**.

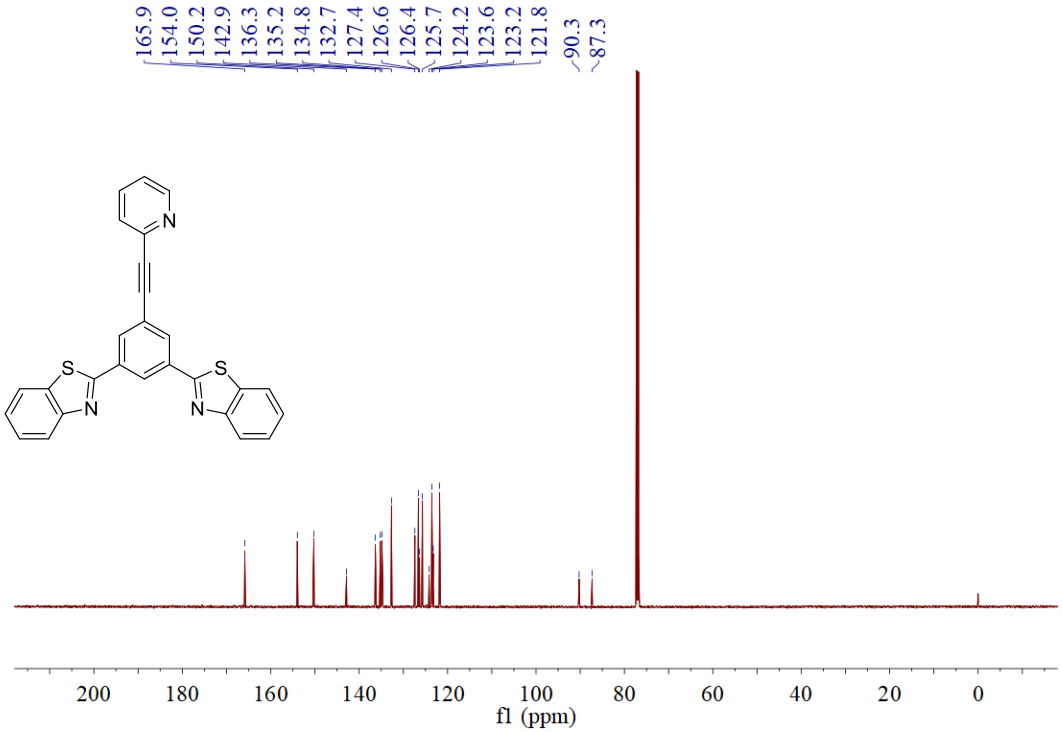

Fig. S13. ^{13}C NMR spectrum of compound **3d**.

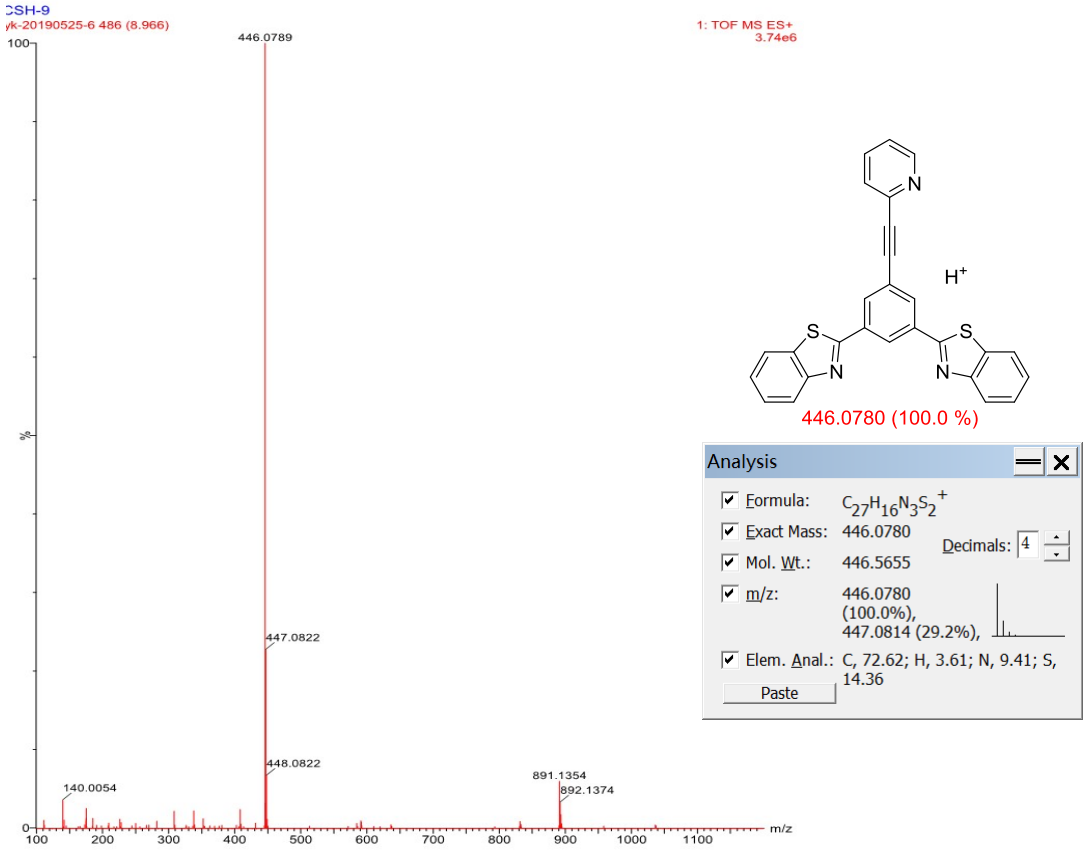

Fig. S14. HRMS spectrum of compound **3d**.

2. UV-*vis* absorption spectra of compounds 3a-3d in THF

The 10^{-5} M solution was prepared with 10^{-3} M stock solution for compounds **3a-3d** respectively. After that, these four solutions were conducted to the UV-*vis* absorption measurement. The results were presented in the following as **Fig. S15**.

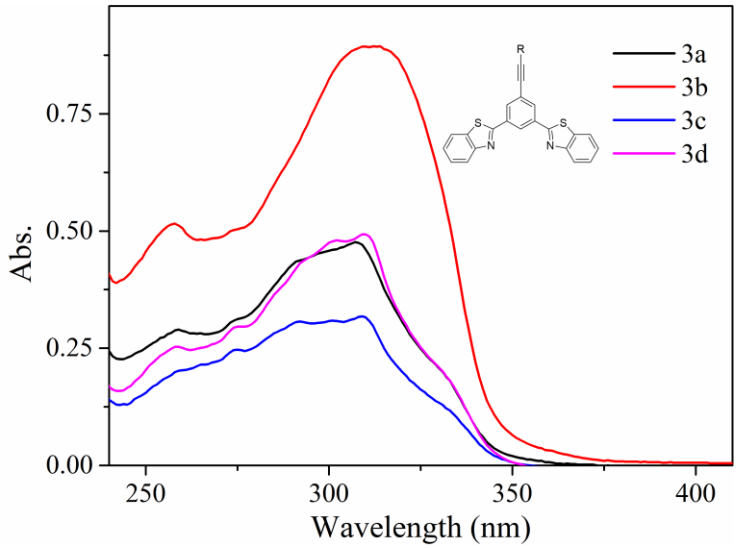

Fig. S15. UV-*vis* absorption spectra of compounds **3a-3d** (10^{-5} M) dissolved in THF.

As shown in **Fig. S15**, their clear absorption band at 310 nm belongs to π-π* transition on aromatic rings and carbon-carbon triple bond.

3. Solid fluorescence spectra of compounds 3a-3d

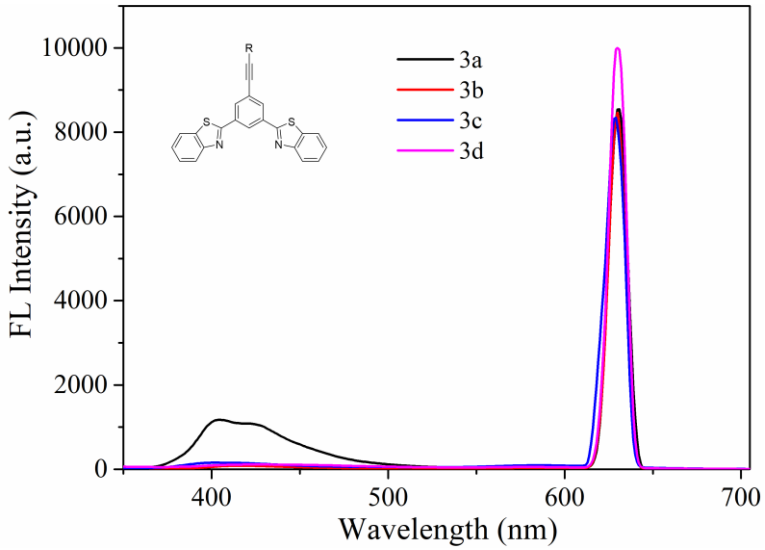

Fig. S16. Solid fluorescence emission spectra of compounds **3a-3d**.

4. Photophysical properties of compounds 3a-3d

Table S1. Photophysical properties of compound **3a-3d** in solvent and solid state.

Title	Solution (THF, 10^{-5} M)			Solid		α_{AIE} [e]	Photo images	
Compounds	λ_{abs} [a] (nm)	λ_{em} [b] (nm)	$\Delta\upsilon$ [c] (nm)	λ_{em} [b]	Φ_f [d]		Solution	Powder
3a	308	386	78	635	1.33	456	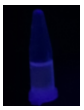	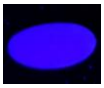
3b	312	409	97	635	4.15	1834		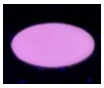
3c	310	384	74	635	1.04	412		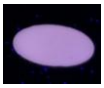
3d	310	379	69	635	2.34	200		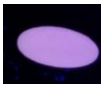

[a] Experimental absorption maxima.
[b] Experimental emission maxima.
[c] Stokes shift.
[d] The fluorescence quantum yields.
[e] Ratio of fluorescence intensity at a moisture content of 90% and a moisture content of 0%.

5. Theoretical calculation of compounds 3a-3d

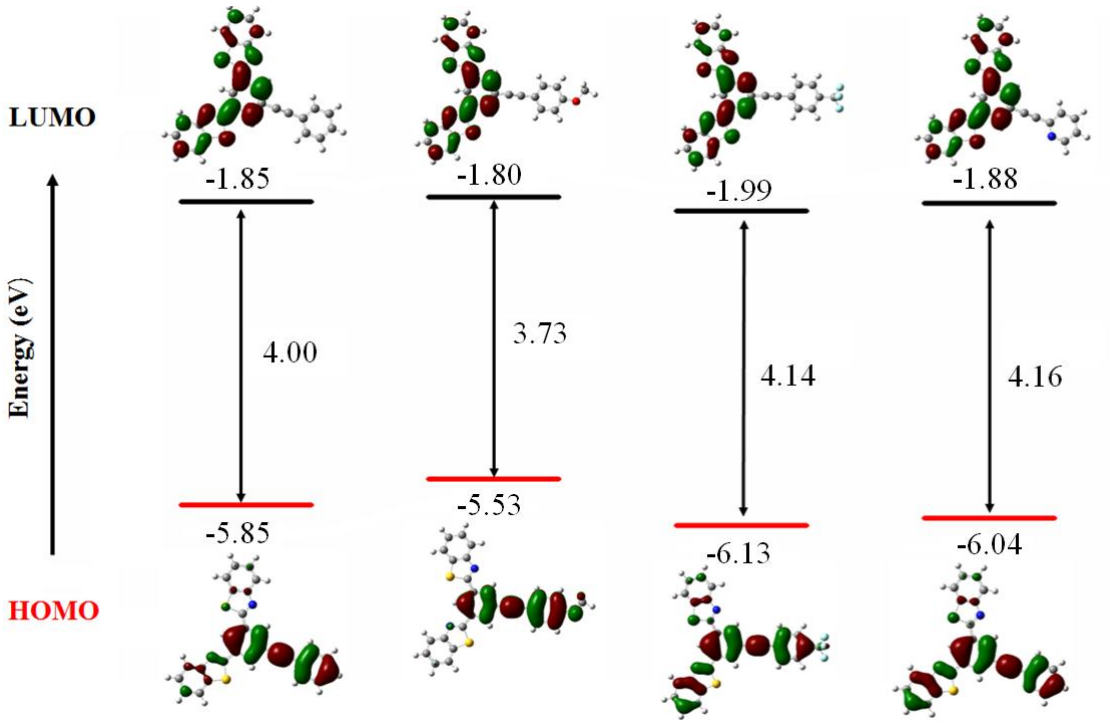

Fig. S17. HOMO-LUMOs of compounds **3a-3d** optimized by the DFT methods.

6. Computational result of optimized structure of 3a-3d

Table S2. Computational result of optimized structure of **3a**.

Center Number	Atomic Number	Coordinates (Angstroms)		
		X	Y	Z
1	6	0.366440	-1.457051	0.000014
2	6	-0.948953	-0.983100	0.000031
3	6	-1.182492	0.401375	0.000060
4	6	-0.115142	1.304884	0.000070
5	6	1.201427	0.819449	0.000069
6	6	1.452556	-0.561316	0.000041
7	6	2.790162	-1.053288	0.000023
8	6	-2.106166	-1.891031	0.000030
9	6	-0.329496	2.760658	0.000101
10	7	0.636176	3.628639	0.000585
11	6	0.160936	4.925661	0.000396
12	6	-1.250227	5.054361	-0.000242
13	16	-1.974880	3.460600	-0.000512
14	16	-1.900763	-3.667833	0.000289
15	6	-3.644584	-3.827026	0.000124
16	6	-4.230607	-2.536986	-0.000091
17	7	-3.338451	-1.482340	-0.000134
18	6	-4.427566	-4.983309	0.000184
19	6	-5.812426	-4.836064	0.000027
20	6	-6.406906	-3.561628	-0.000188
21	6	-5.628346	-2.411455	-0.000249
22	6	0.961424	6.078448	0.000757
23	6	0.347018	7.324052	0.000480
24	6	-1.054705	7.437757	-0.000158
25	6	-1.867640	6.307065	-0.000528
26	6	3.930669	-1.474799	-0.000018
27	6	5.270194	-1.961166	-0.000076
28	6	5.530704	-3.346196	0.000310
29	6	6.841409	-3.814924	0.000252
30	6	7.911292	-2.916311	-0.000195
31	6	7.663530	-1.541217	-0.000587
32	6	6.356326	-1.062995	-0.000529
33	1	0.572878	-2.522718	-0.000033
34	1	-2.212403	0.742119	0.000108

35	1	2.024075	1.524439	0.000101
36	1	-3.973788	-5.969631	0.000350
37	1	-6.441467	-5.721750	0.000072
38	1	-7.489875	-3.477588	-0.000308
39	1	-6.072069	-1.420948	-0.000416
40	1	2.041789	5.974229	0.001246
41	1	0.955733	8.223729	0.000764
42	1	-1.513248	8.422597	-0.000352
43	1	-2.949339	6.400342	-0.000993
44	1	4.696722	-4.041281	0.000668
45	1	7.029151	-4.885200	0.000559
46	1	8.933077	-3.285762	-0.000246
47	1	8.492445	-0.838629	-0.000935
48	1	6.159546	0.004612	-0.000825

Table S3. Computational result of optimized structure of **3b**.

Center Number	Atomic Number	Coordinates (Angstroms)		
		X	Y	Z
1	6	-3.504992	-0.404720	-0.000238
2	6	-2.294400	-0.285326	-0.000165
3	6	-0.876575	-0.147301	-0.000138
4	6	-0.051087	-1.288051	-0.000118
5	6	1.341480	-1.162539	-0.000117
6	6	1.918503	0.117385	-0.000123
7	6	1.113622	1.261092	-0.000145
8	6	-0.282913	1.124810	-0.000146
9	6	2.229798	-2.334737	-0.000059
10	6	1.689133	2.615287	-0.000168
11	16	1.577393	-4.000495	-0.001621
12	6	3.222592	-4.599786	-0.000336
13	6	4.118742	-3.502238	0.000848
14	7	3.525638	-2.254598	0.000934
15	7	0.975583	3.700121	0.000462
16	6	1.764461	4.834095	0.000345
17	6	3.162096	4.600536	-0.000481
18	16	3.458830	2.875362	-0.001211
19	6	3.684134	-5.917695	-0.000484
20	6	5.060636	-6.129529	0.000558
21	6	5.960994	-5.049351	0.001746
22	6	5.502156	-3.738380	0.001910
23	6	1.282722	6.152275	0.001006

24	6	2.192963	7.201352	0.000819
25	6	3.577666	6.955729	-0.000007
26	6	4.077013	5.655736	-0.000659
27	6	-4.921731	-0.538857	-0.000221
28	6	-5.531330	-1.813347	-0.000483
29	6	-6.910002	-1.941497	-0.000380
30	6	-7.728167	-0.799619	-0.000077
31	6	-7.141611	0.473104	0.000203
32	6	-5.753779	0.594357	0.000137
33	8	-9.069318	-1.035204	-0.000147
34	6	-9.950962	0.077991	0.001368
35	1	-0.520234	-2.266932	-0.000075
36	1	3.001067	0.186776	-0.000060
37	1	-0.900186	2.015165	-0.000138
38	1	2.993193	-6.755174	-0.001441
39	1	5.442271	-7.146631	0.000425
40	1	7.029519	-5.244728	0.002541
41	1	6.184450	-2.894263	0.002836
42	1	0.211235	6.325470	0.001650
43	1	1.832405	8.226044	0.001313
44	1	4.271140	7.791978	-0.000149
45	1	5.147033	5.471689	-0.001309
46	1	-4.904925	-2.699991	-0.000749
47	1	-7.384179	-2.917842	-0.000544
48	1	-7.751178	1.369284	0.000459
49	1	-5.302515	1.581751	0.000331
50	1	-10.959001	-0.340077	0.002124
51	1	-9.814411	0.698471	0.896602
52	1	-9.816222	0.699438	-0.893474

Table S4. Computational result of optimized structure of **3c**.

1	6	-0.442030	-1.223676	-0.012502
2	6	-1.839896	-1.206986	-0.006061
3	6	-2.513217	0.025221	-0.002748
4	6	-1.801758	1.229157	-0.005848
5	6	-0.398779	1.202138	-0.012594
6	6	0.288984	-0.020729	-0.015828
7	6	1.714147	-0.048590	-0.021763
8	6	-2.635853	-2.443996	-0.002518
9	6	-2.481235	2.534471	-0.001739
10	7	-1.851646	3.670099	-0.004384

11	6	-2.724674	4.740620	0.001261
12	6	-4.100324	4.400894	0.008582
13	16	-4.264064	2.657798	0.008172
14	16	-1.860150	-4.054866	-0.005433
15	6	-3.455843	-4.776233	0.001349
16	6	-4.431911	-3.749127	0.005225
17	7	-3.933929	-2.460527	0.002918
18	6	-3.816741	-6.125179	0.003007
19	6	-5.173522	-6.439151	0.008597
20	6	-6.152604	-5.429617	0.012491
21	6	-5.793814	-4.087943	0.010871
22	6	-2.344960	6.091786	0.000371
23	6	-3.332832	7.067867	0.006719
24	6	-4.694793	6.717037	0.013910
25	6	-5.093478	5.382807	0.014919
26	6	2.929507	-0.077628	-0.026038
27	6	4.353099	-0.108681	-0.029178
28	6	5.043499	-1.337086	-0.013003
29	6	6.433091	-1.364953	-0.015699
30	6	7.158169	-0.169952	-0.036419
31	6	6.485521	1.056029	-0.054967
32	6	5.096360	1.088856	-0.051781
33	6	8.661077	-0.198965	0.021625
34	9	9.164640	-1.334221	-0.511578
35	9	9.112903	-0.129745	1.296303
36	9	9.209832	0.841996	-0.643608
37	1	0.102591	-2.162575	-0.015056
38	1	-3.597942	0.009394	0.002387
39	1	0.147425	2.137796	-0.014876
40	1	-3.065083	-6.908543	0.000021
41	1	-5.478009	-7.481916	0.009964
42	1	-7.203291	-5.705034	0.016834
43	1	-6.537476	-3.297437	0.013824
44	1	-1.289972	6.346735	-0.005199
45	1	-3.051756	8.117092	0.006148
46	1	-5.450043	7.497841	0.018798
47	1	-6.146189	5.117312	0.020545
48	1	4.478513	-2.263466	-0.000650
49	1	6.957901	-2.314363	-0.009000
50	1	7.050522	1.982101	-0.079201
51	1	4.571747	2.038550	-0.069603

Table S5. Computational result of optimized structure of **3d**.

Center Number	Atomic Number	Coordinates (Angstroms)		
		X	Y	Z
1	6	0.374364	-1.457158	-0.000036
2	6	-0.939966	-0.980663	0.000025
3	6	-1.170180	0.404601	0.000076
4	6	-0.102228	1.307258	-0.000010
5	6	1.213616	0.819545	-0.000072
6	6	1.460360	-0.561347	-0.000064
7	6	2.795875	-1.059406	-0.000084
8	6	-2.099618	-1.885748	0.000103
9	6	-0.314527	2.763247	-0.000008
10	7	0.652868	3.629446	0.001456
11	6	0.179805	4.927273	0.000984
12	6	-1.231150	5.058263	-0.000969
13	16	-1.958454	3.465727	-0.002246
14	16	-1.899668	-3.662095	-0.001397
15	6	-3.643799	-3.815490	-0.000383
16	6	-4.226005	-2.523675	0.000947
17	7	-3.330466	-1.472008	0.001167
18	6	-4.430307	-4.969476	-0.000736
19	6	-5.814609	-4.817905	0.000269
20	6	-6.405337	-3.541605	0.001603
21	6	-5.623422	-2.393812	0.001951
22	6	0.982111	6.078819	0.002284
23	6	0.369673	7.325363	0.001598
24	6	-1.031888	7.441289	-0.000362
25	6	-1.846621	6.311924	-0.001656
26	6	3.925245	-1.506837	-0.000133
27	6	5.267039	-2.001936	-0.000062
28	7	5.433122	-3.342716	0.000287
29	6	6.684546	-3.805696	0.000403
30	6	7.821616	-2.993194	0.000176
31	6	7.643165	-1.610231	-0.000206
32	6	6.348680	-1.101242	-0.000333
33	1	0.581634	-2.522604	0.000013
34	1	-2.199677	0.746803	0.000247
35	1	2.037532	1.523090	-0.000110
36	1	-3.979420	-5.957101	-0.001757
37	1	-6.446373	-5.701649	0.000020
38	1	-7.488060	-3.454419	0.002370
39	1	-6.064163	-1.401966	0.002983
40	1	2.062321	5.972976	0.003792

41	1	0.979767	8.224098	0.002585
42	1	-1.488847	8.426853	-0.000869
43	1	-2.928163	6.406898	-0.003155
44	1	6.786177	-4.889995	0.000690
45	1	8.813005	-3.435916	0.000297
46	1	8.497204	-0.938408	-0.000399
47	1	6.159728	-0.032782	-0.000625

7. UV-*vis* absorption and fluorescence spectra of compound 3a in various solvents

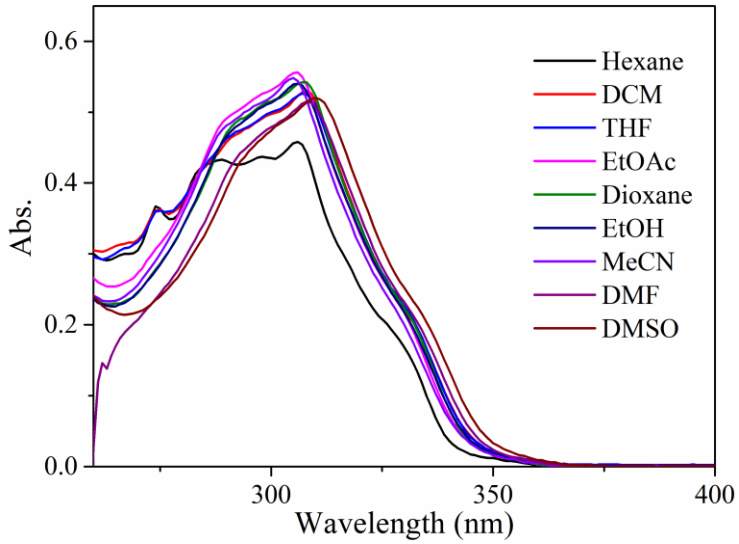

Fig. S18. UV-*vis* absorption spectra of compound **3a** (10^{-5} M) in various solvents.

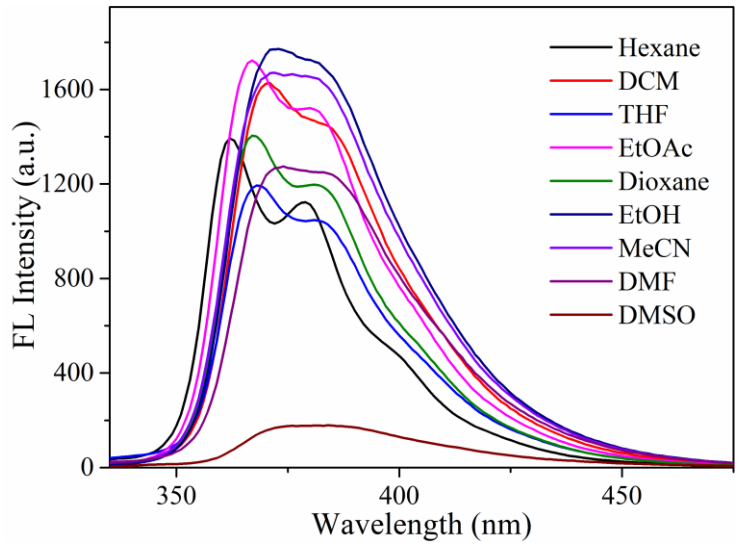

Fig. S19. Fluorescence spectra of compound **3a** (10^{-5} M) in various solvents.

8. UV-*vis* absorption and fluorescence spectra of compound 3c in various solvents

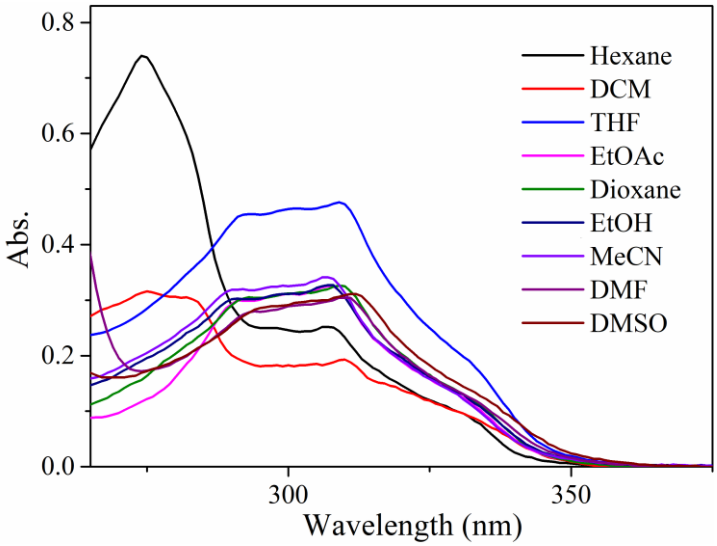

Fig. S20. UV-*vis* absorption spectra of compound **3c** (10^{-5} M) in various solvents.

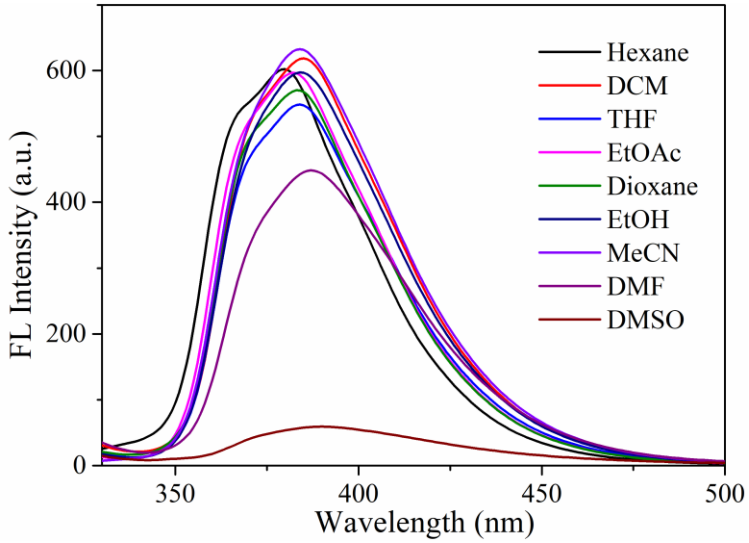

Fig. S21. Fluorescence spectra of compound **3c** (10^{-5} M) in various solvents.

9. UV-*vis* absorption and fluorescence spectra of compound 3d in various solvents

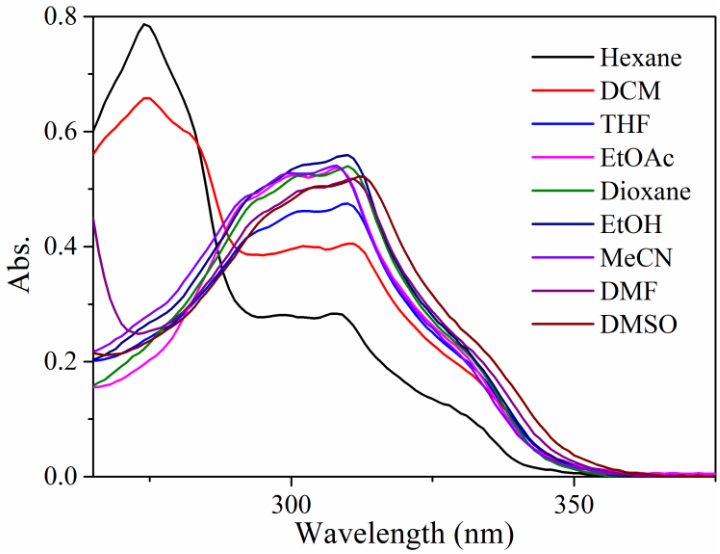

Fig. S22. UV-*vis* absorption spectra of compound **3d** (10^{-5} M) in various solvents.

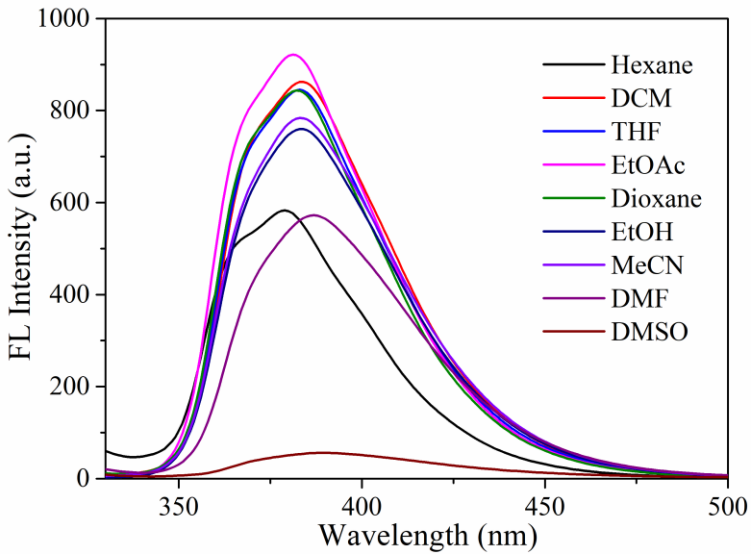

Fig. S23. Fluorescence spectra of compound **3d** (10^{-5} M) in various solvents.

10. UV-*vis* absorption spectra of compound 3b

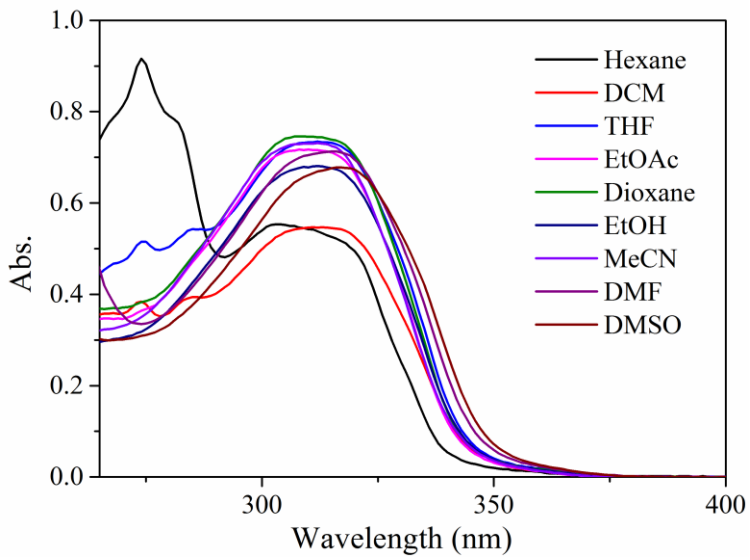

Fig. S24. UV-*vis* absorption spectra of compound **3b** (10^{-5} M) in various solvents.

11. Lippert-Mataga plots of compound 3b

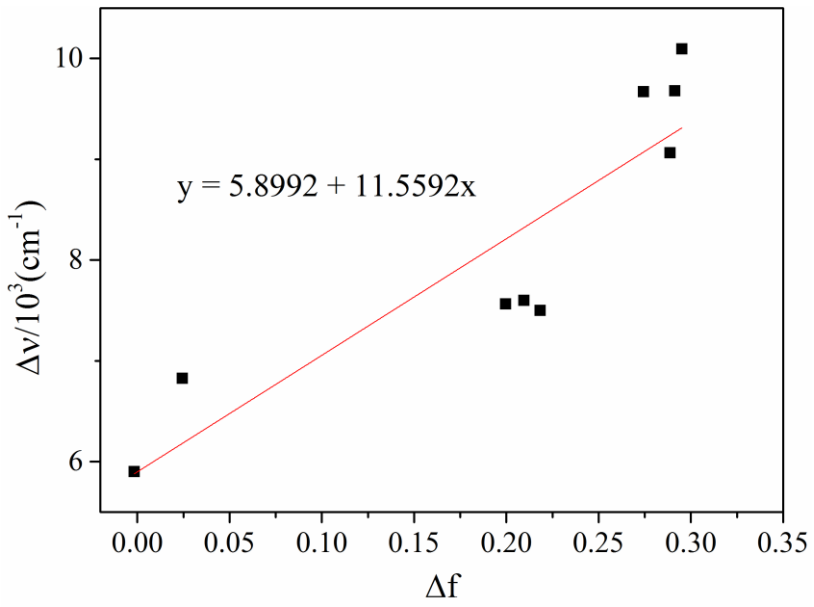

Fig. S25. Lippert-Mataga plots of compound **3b** (10^{-5} M) in various solvents.

12. Photophysical properties of compound 3b

Table S6. Photophysical properties of compound **3b** in solvents and solid state.

Conditions	λ_{abs} [a] (nm)	λ_{em} [b] (nm)	$\Delta\upsilon$ [c] (cm^{-1})	Φx [d]	CIE [e] (x, y)
Hexane	303	369	5903	0.93	0.1575, 0.421
DCM	313	409	7499	0.41	0.1700, 0.0193
THF	312	409	7601	0.50	0.1575, 0.0421
EtOAc	310	405	7566	0.52	0.1580, 0.0441
Dioxane	308	390	6826	0.57	0.1567, 0.0464
EtOH	312	435	9062	0.31	0.1622, 0.0243
MeCN	312	447	9679	0.23	0.1563, 0.1090
DMF	315	453	9670	0.27	0.1604, 0.1547
DMSO	316	464	10093	0.10	0.1693, 0.2021
Solid	312	635	16178	-	0.6631, 0.2878

[a] Experimental absorption maxima.

[b] Experimental emission maxima.

[c] Stokes shift.

[d] The relatively fluorescence quantum yields, taking quinine sulfate as the standard substance ($\Phi s = 0.54$).

[e] CIE color coordinate for the emission at 298 K.

13. The fluorescence and absorption spectra of compound 3a in H_2O/THF system

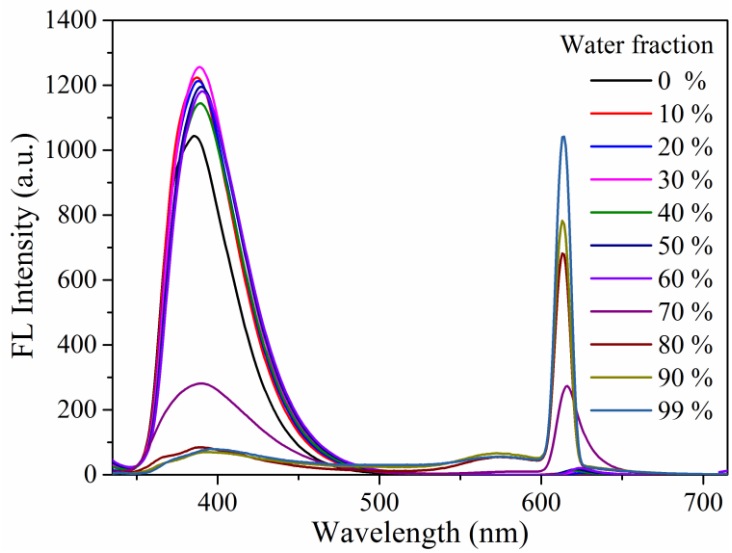

Fig. S26. The fluorescence spectra of compound **3a** (10^{-5} M) in H_2O/THF system with different water fractions (f_w).

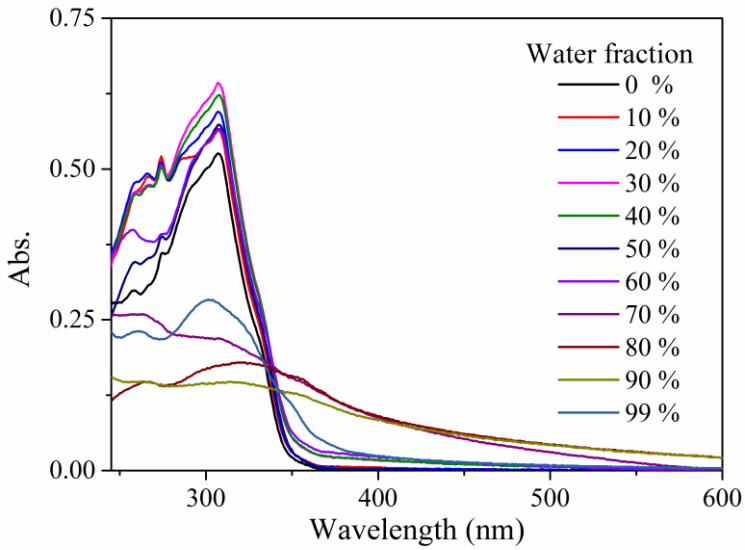

Fig. S27. The UV-*vis* absorption spectra of compound **3a** (10^{-5} M) in H_2O/THF system with different water fractions (f_w).

14. The fluorescence and absorption spectra of compound 3c in H_2O/THF system

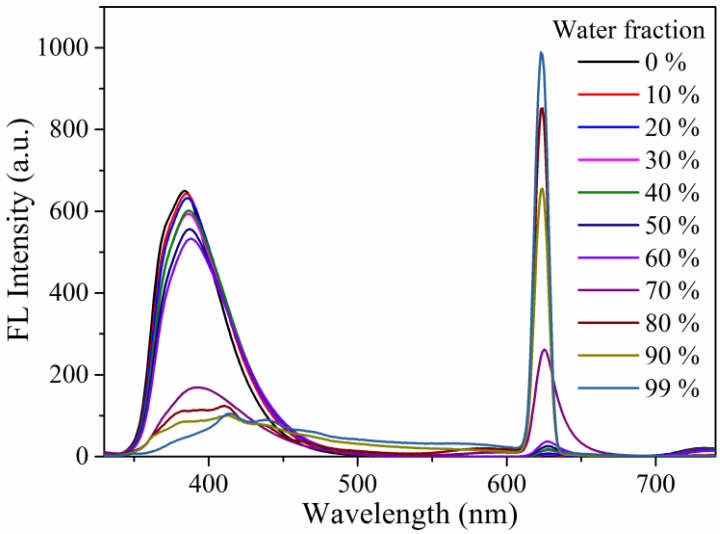

Fig. S28. The fluorescence spectra of compound **3c** (10^{-5} M) in H_2O/THF system with different water fractions (f_w).

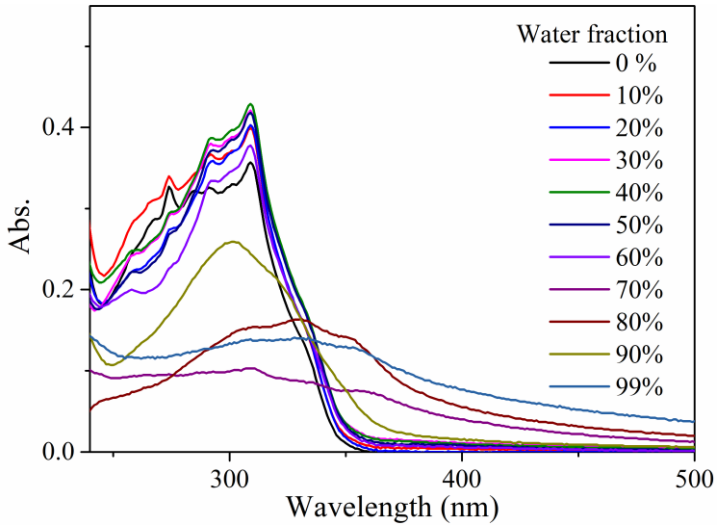

Fig. S29. The UV-*vis* absorption spectra of compound **3c** (10^{-5} M) in H_2O/THF system with different water fractions (f_w).

15. The fluorescence and absorption spectra of compound 3d in H_2O/THF system

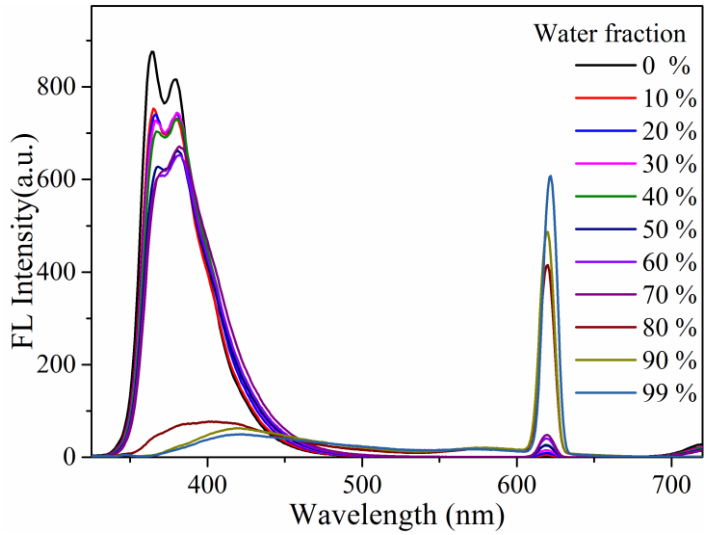

Fig. S30. The fluorescence spectra of compound **3d** (10^{-5} M) in H_2O/THF system with different water fractions (f_w).

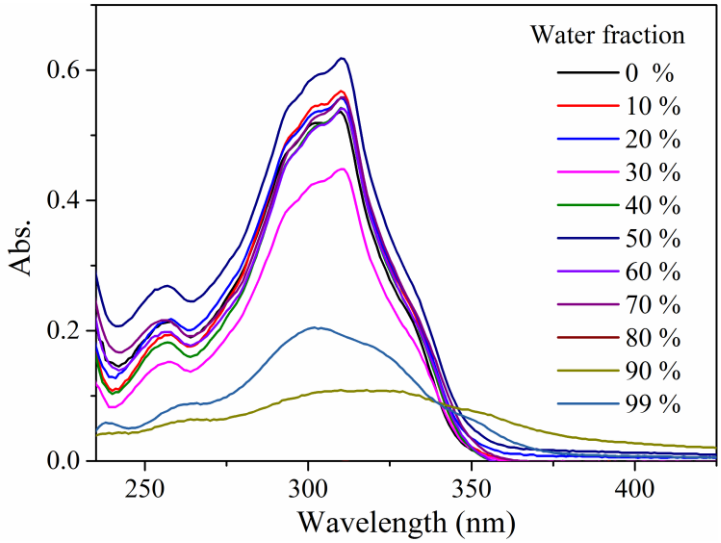

Fig. S31. The UV-*vis* absorption spectra of compound **3d** (10^{-5} M) in H_2O/THF system with different water fractions (f_w).

16. Scanning electron micrograph (SEM) of compounds 3a, 3c and 3d

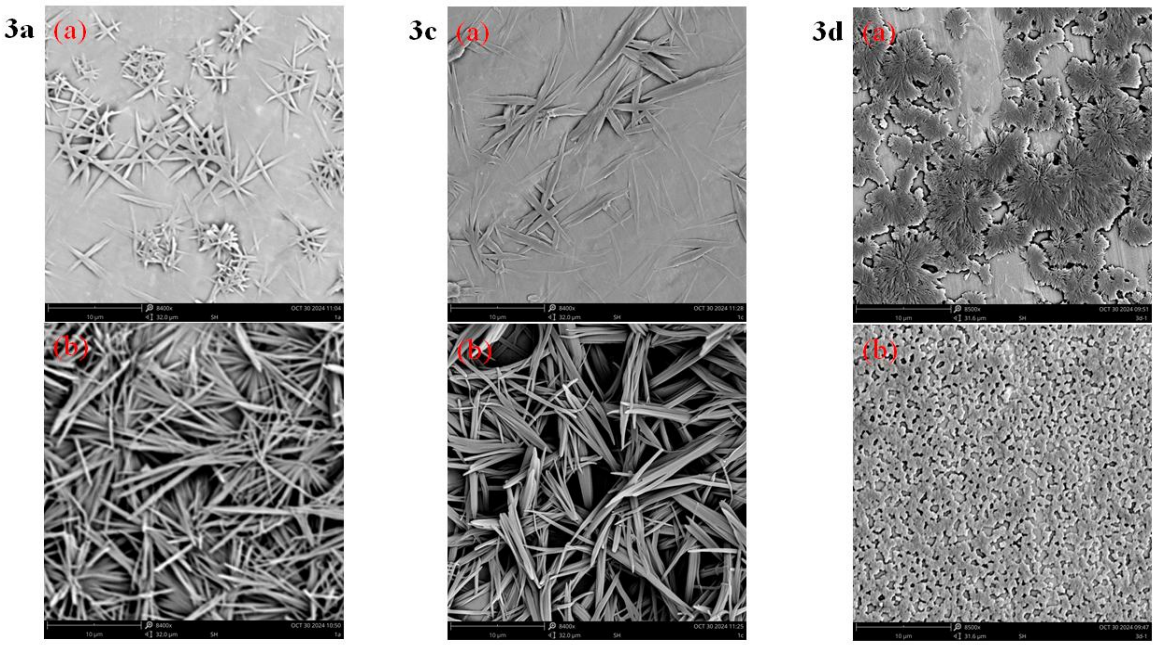

Fig. S32. Scanning electron micrograph (SEM) of compounds **3a**, **3c** and **3d** (a) 10^{-3} M (THF) and (b) supersaturated concentration.

17. Structures of other NACs in selectivity studies

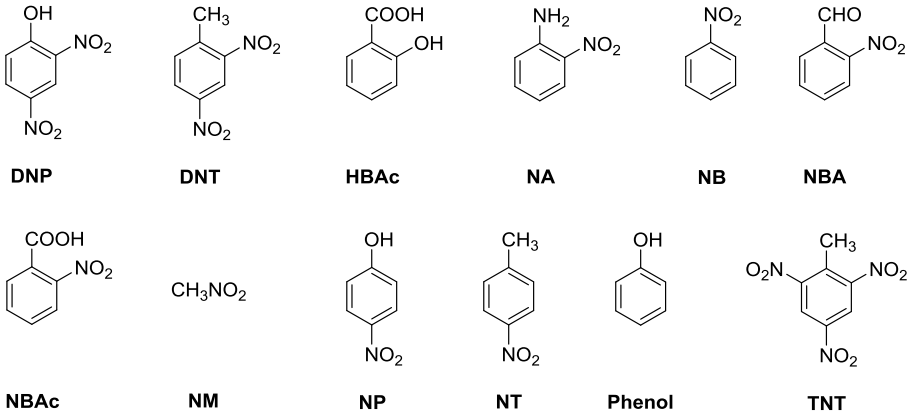

Fig. S33. Structures of the other NACs in selectivity studies.

18. Fluorescence spectra of selectivity study for 3b towards different NACs

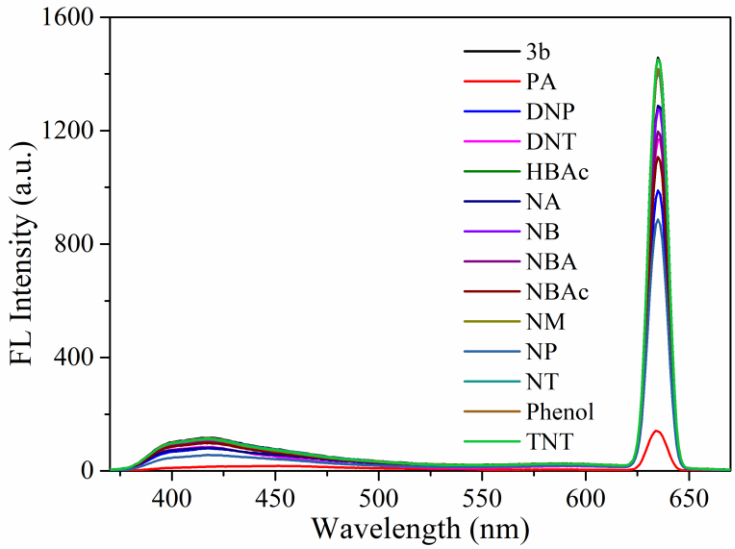

Fig. S34. Fluorescence spectra of compound **3b** (10^{-5} M in H_2O/THF, v/v, 9/1) with 5 equiv. different aromatic explosives.

19. Fluorescence spectra of selectivity study for 3b towards different metal ions

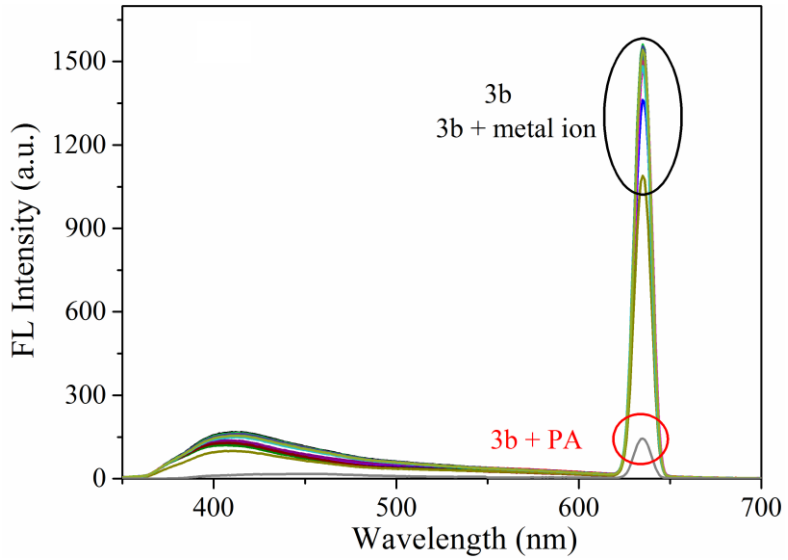

Fig. S35. Fluorescence spectra of compound **3b** (10^{-5} M in H_2O/THF, v/v, 9/1) with 5 equiv. different metal ions.

20. Fluorescence spectra of selectivity study for 3b towards different anions

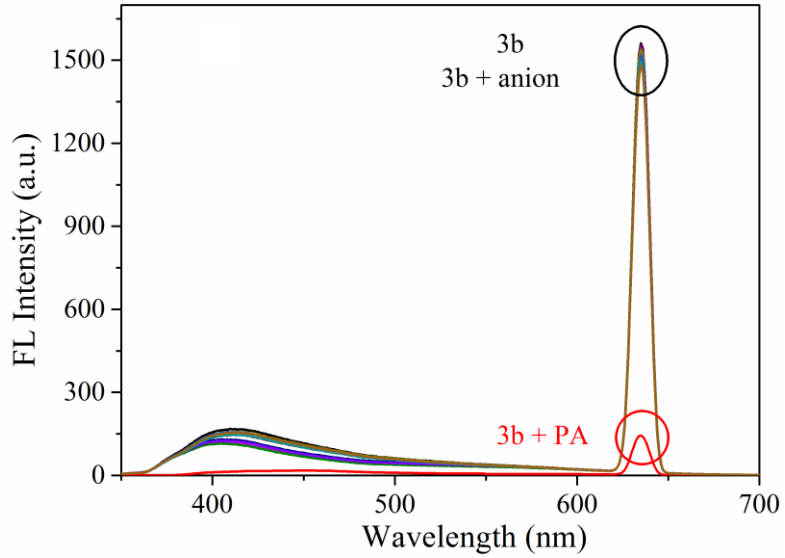

Fig. S36. Fluorescence spectra of compound **3b** (10^{-5} M in H_2O/THF, v/v, 9/1) with 5 equiv. different anions.

21. Relationship between fluorescence intensity of 3a and the amount of PA

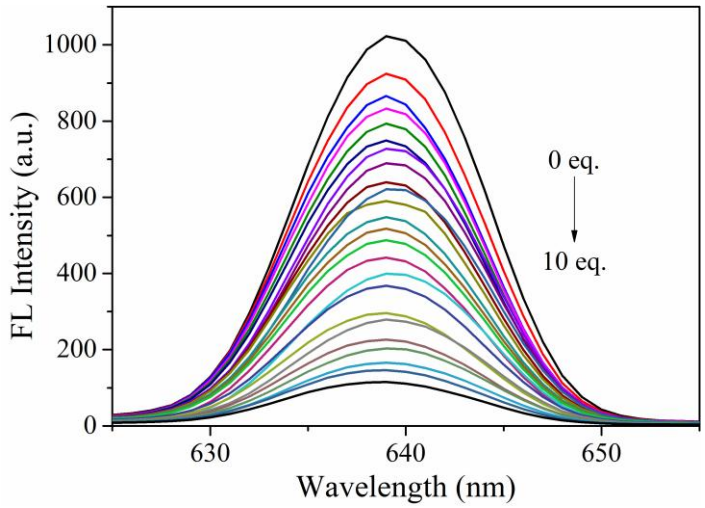

Fig. S37. Fluorescence spectra of compound **3a** (10^{-5} M) upon the addition of different equivalents of PA dissolved in H_2O/THF (v/v, 9/1).

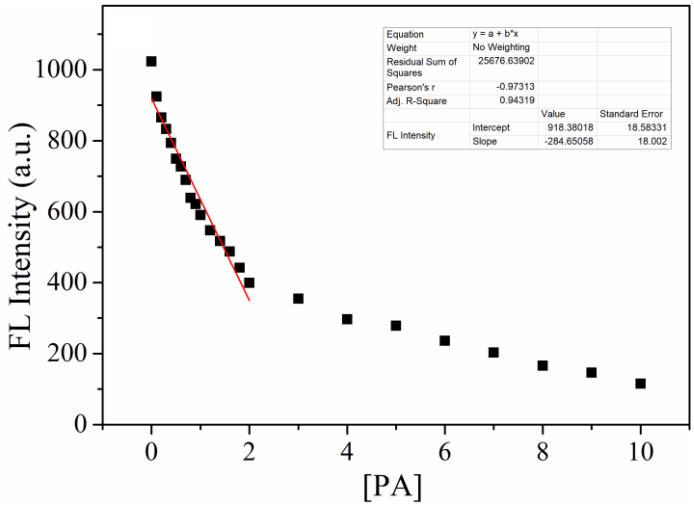

Fig. S38. Relation between the maximum fluorescence intensity of **3a** (10^{-5} M in H_2O/THF, v/v, 9/1) and equivalent of PA (1-10 eq.).

22. Relationship between fluorescence intensity of 3c and the amount of PA

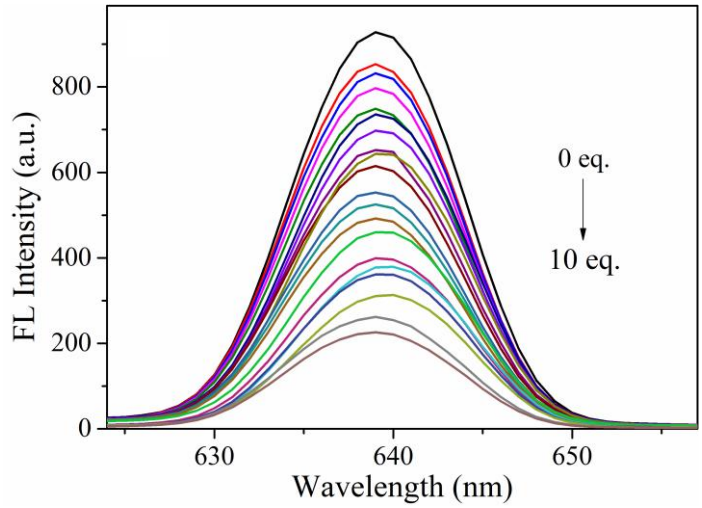

Fig. S39. Fluorescence spectra of compound **3c** (10^{-5} M) upon the addition of different equivalents of PA dissolved in H_2O/THF (v/v, 9/1).

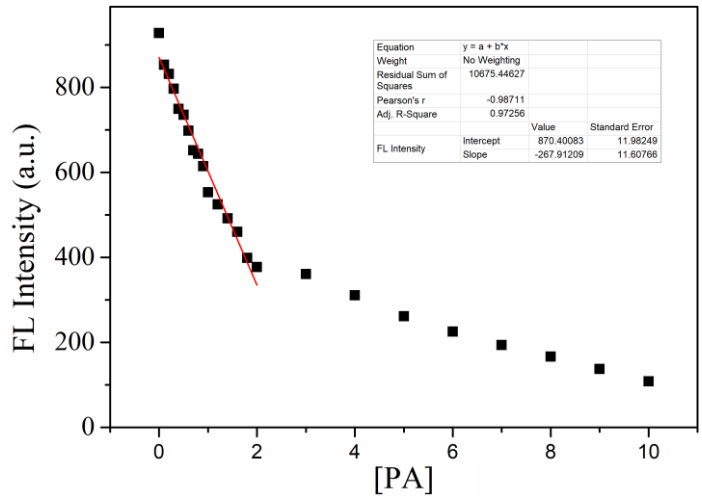

Fig. S40. Relation between the maximum fluorescence intensity of **3c** (10^{-5} M in H_2O/THF, v/v, 9/1) and equivalent of PA (1-10 eq.).

23. Relationship between fluorescence intensity of 3d and the amount of PA

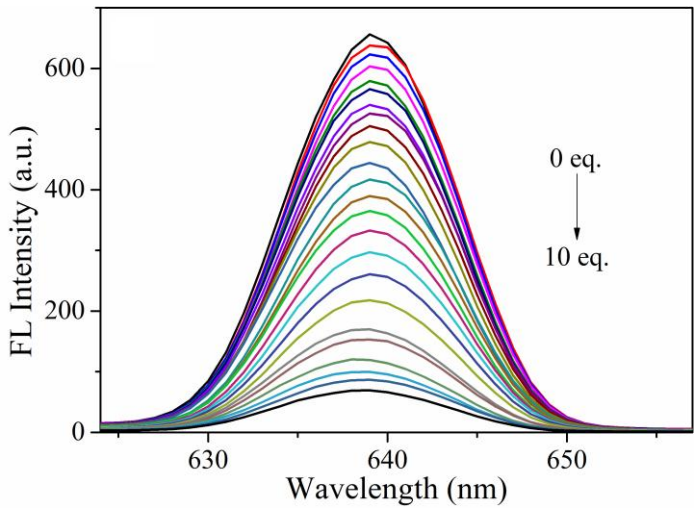

Fig. S41. Fluorescence spectra of compound **3d** (10^{-5} M) upon the addition of different equivalents of PA dissolved in H_2O/THF (v/v, 9/1).

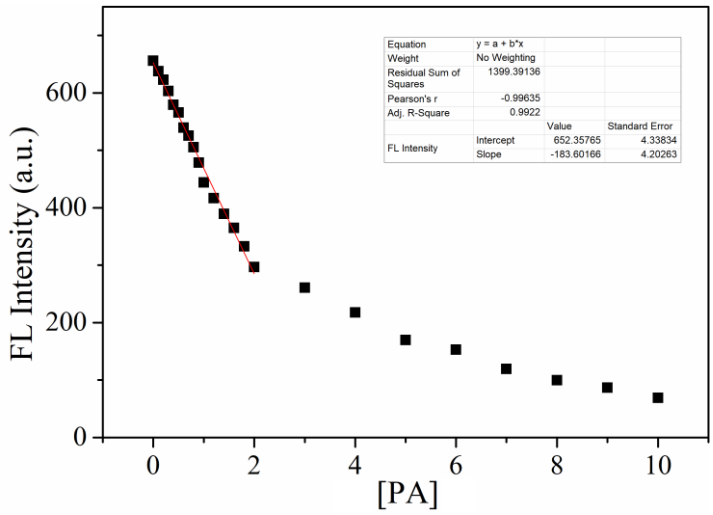

Fig. S42. Relation between the maximum fluorescence intensity of **3d** (10^{-5} M in H_2O/THF, v/v, 9/1) and equivalent of PA (1-10 eq.).

24. Stern-Volmer plots of 3b in response to PA

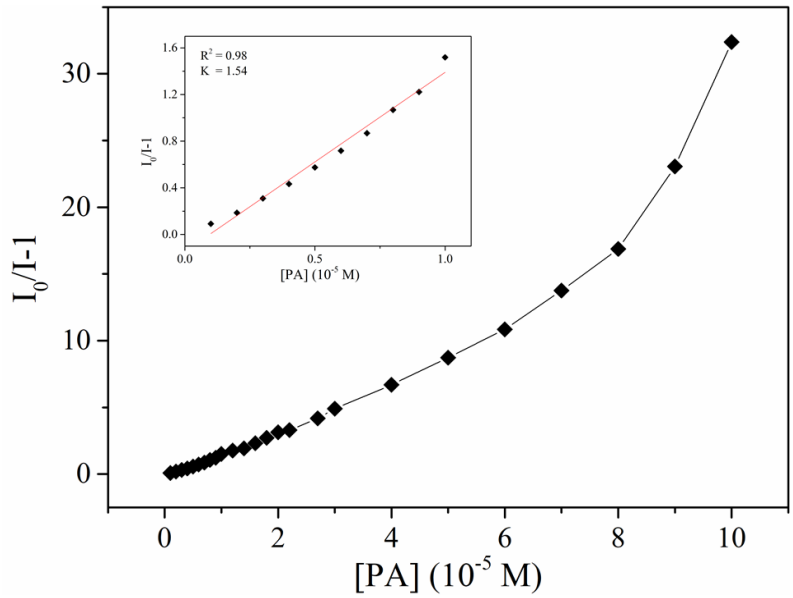

Fig. S43. Stern-Volmer plots of **3b** (10^{-5} M in H_2O/THF, v/v, 9/1) in response to PA. Inset: Stern-Volmer plots obtained at lower concentration of PA.

25. Stern-Volmer plots of 3a in response to PA

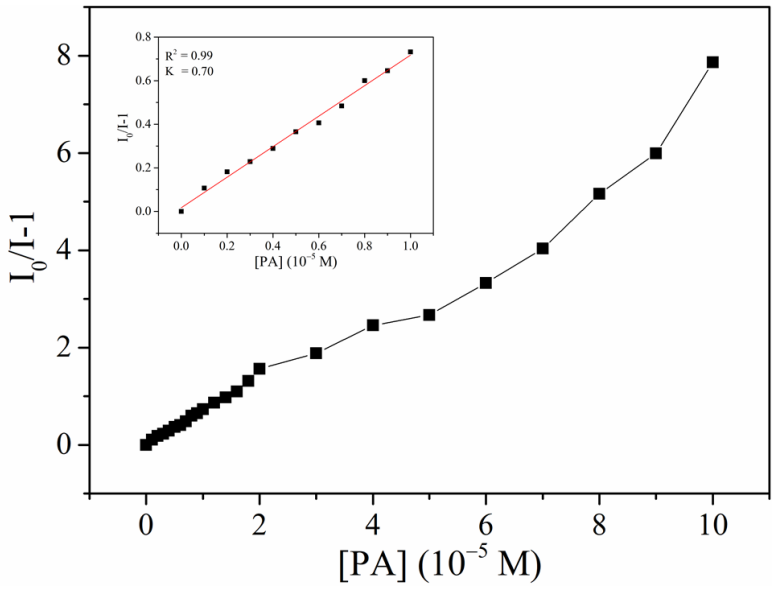

Fig. S44. Stern-Volmer plots of **3a** (10^{-5} M in H_2O/THF, v/v, 9/1) in response to PA. Inset: Stern-Volmer plots obtained at lower concentration of PA.

26. Stern-Volmer plots of 3c in response to PA

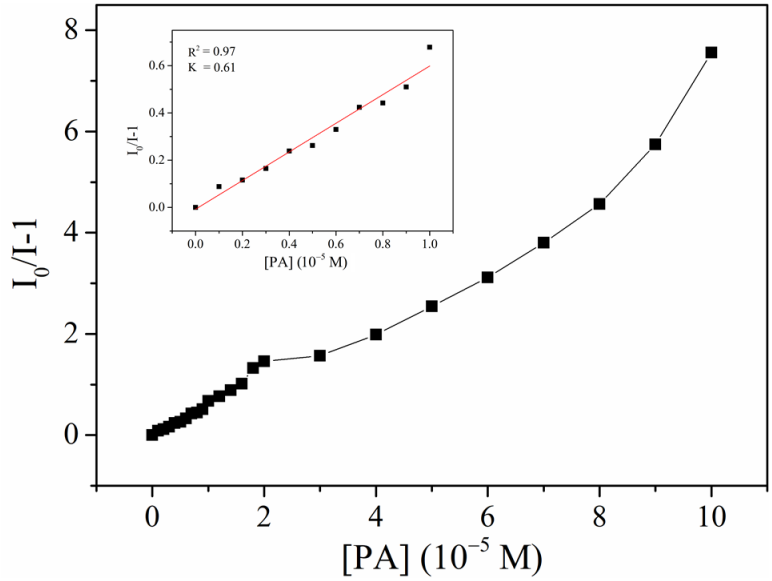

Fig. S45. Stern-Volmer plots of **3c** (10^{-5} M in H_2O/THF, v/v, 9/1) in response to PA. Inset: Stern-Volmer plots obtained at lower concentration of PA.

27. Stern-Volmer plots of 3d in response to PA

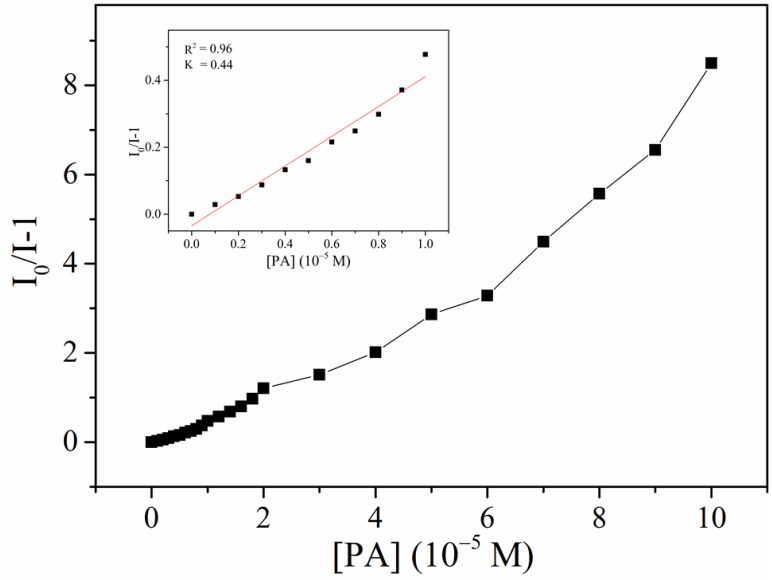

Fig. S46. Stern-Volmer plots of **3d** (10^{-5} M in H_2O/THF, v/v, 9/1) in response to PA. Inset: Stern-Volmer plots obtained at lower concentration of PA.

28. Time-dependent fluorescence intensity of 3b with PA

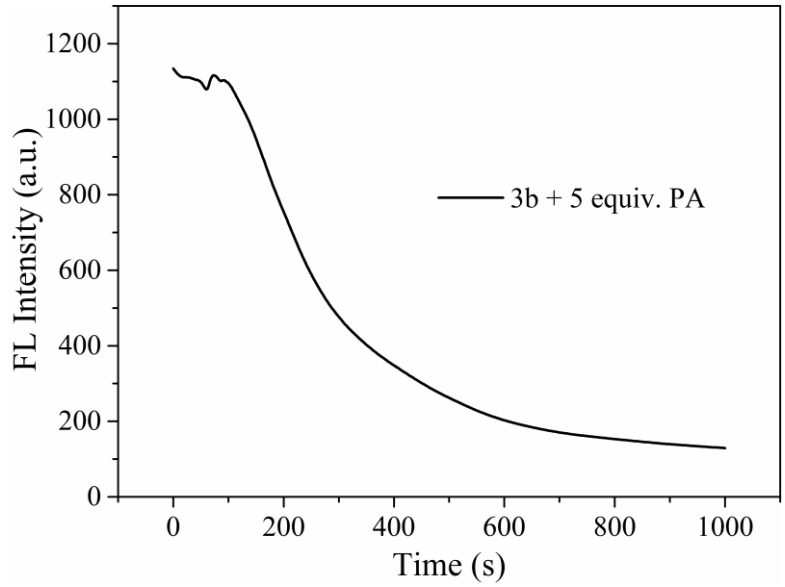

Fig. S47. Time-dependent the maximum emission intensity of **3b** (10^{-5} M in H_2O/THF, v/v, 9/1) upon the addition of 5 equiv. PA.

29. The impact of pH to the fluorescence intensity of 3b with PA

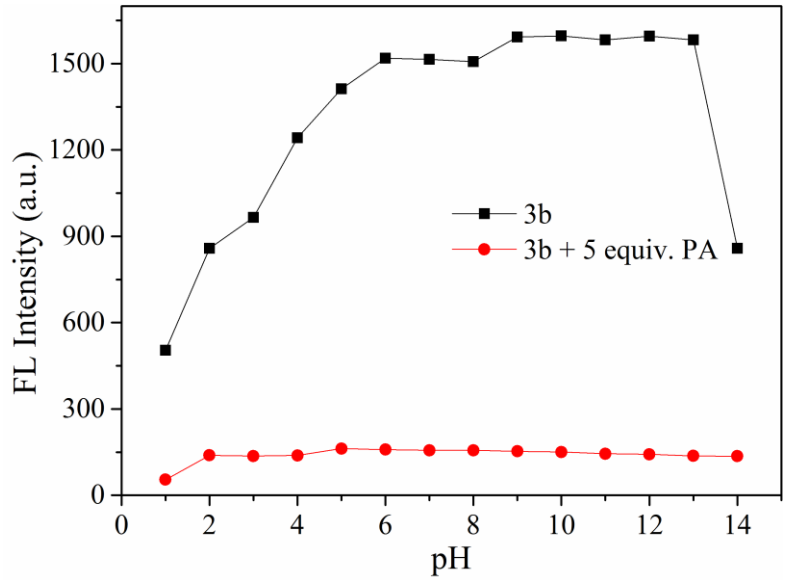

Fig. S48. The maximum fluorescence intensity of **3b** (10^{-5} M in H_2O/THF, v/v, 9/1) before and after the addition of 5 equiv. PA as a function of different pH values.

30. Job's plot for the evolution of binding stoichiometry between 3b and PA

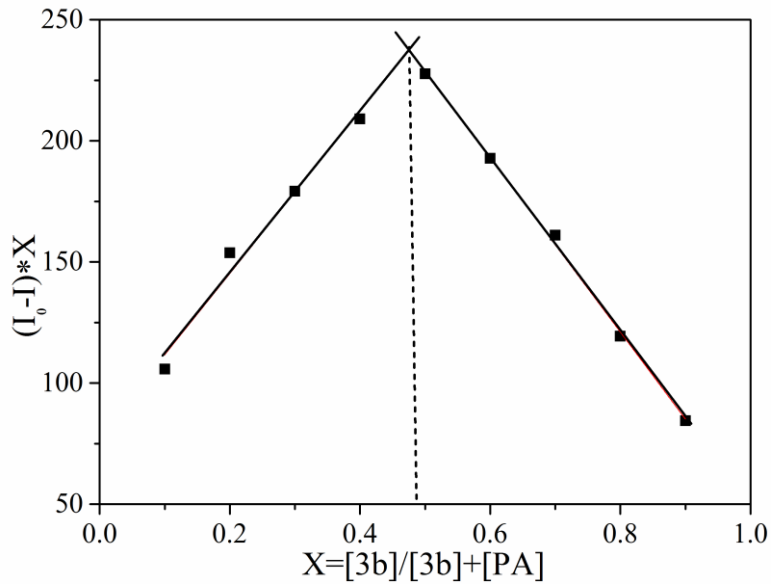

Fig. S49. Job's plot for the evolution of binding stoichiometry between **3b** and PA (in H_2O/THF, v/v, 9/1). The total concentration of PA and [**3b**] was 10^{-5} M.

31. DLS of compound 3b before and after interaction with PA

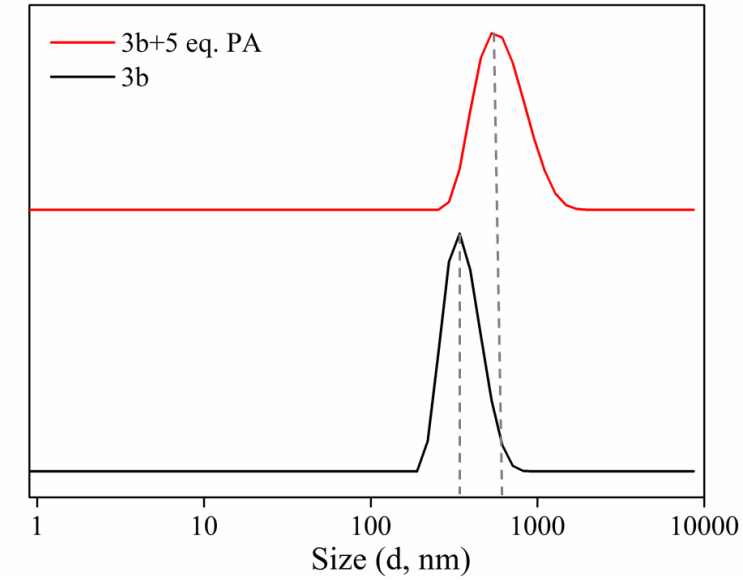

Fig. S50. Size change of compound **3b** (10^{-5} M, H_2O/THF, v/v, 9/1) before and after interaction with 5 equiv. PA.

32. SEM of compound 3b before and after interaction with PA

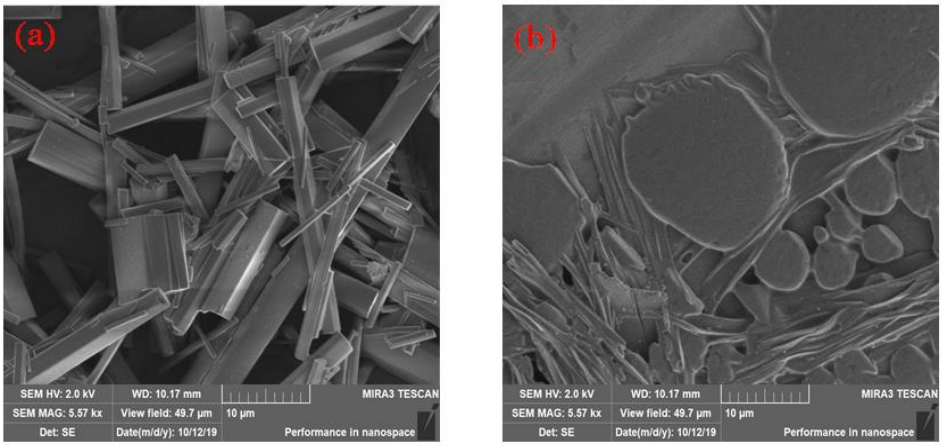

Fig. S51. SEM images of compound **3b** (H_2O/THF, v/v, 9/1) (a) before and (b) after interaction with 5 equiv. PA.

33. TCSPC plot for 3b with PA

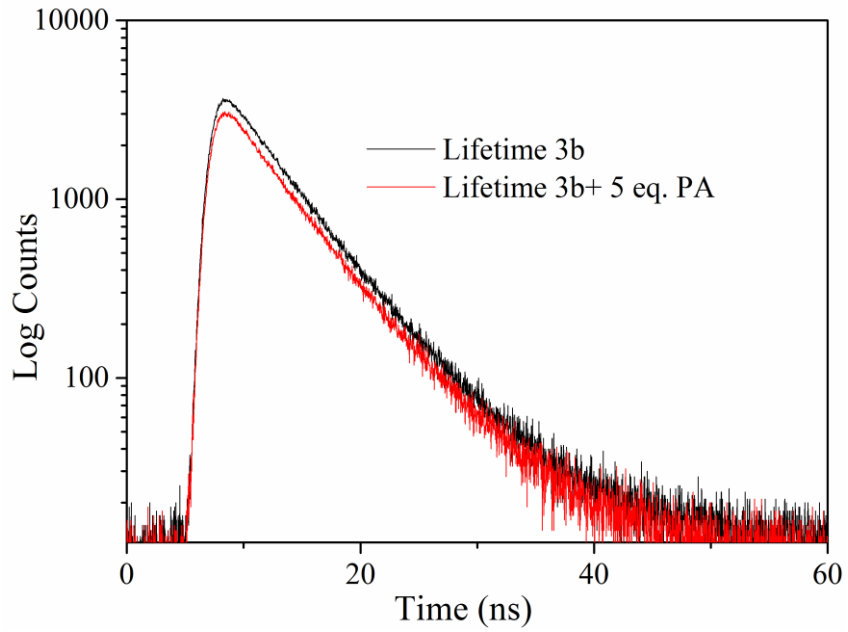

Fig. S52. Time-correlated single photon counting (TCSPC) plot for **3b** (10^{-5} M in H_2O/THF, v/v, 9/1) with 5 eq. PA.

Table S7. Fluorescence lifetime data for **3b** with 5 eq. PA.

Substance in solution	τ (ns)	χ^2
3b	4.9080	1.909
3b + 5 eq. PA	4.8853	2.659

34. The LUMO-HOMO energy levels of 3b, PA and other NACs

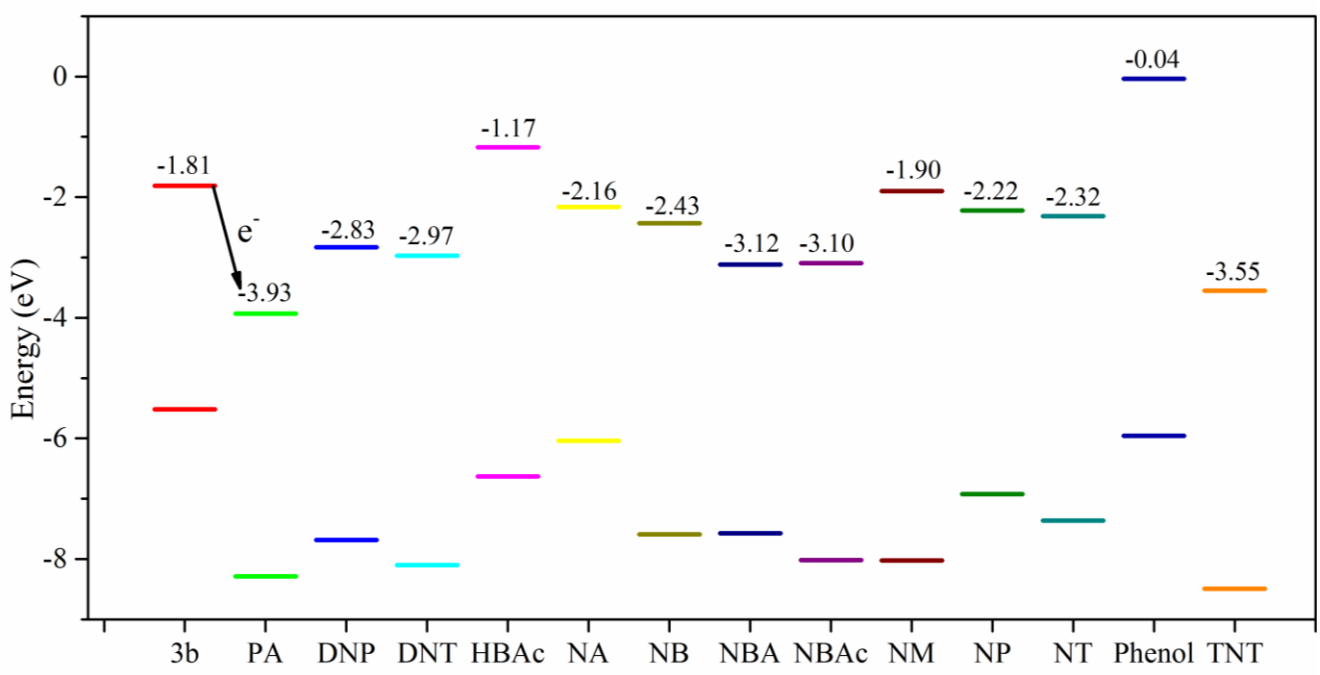

Fig. S53. The LUMO-HOMO energy levels of **3b** and NACs.

35. The comparison of our sensor 3b with other reported PA sensors

Table S8. The comparison of our sensor **3b** with reported PA sensors in solution.

No.	Probe type	Solvent (v/v)	Quenching constant (M^{-1})	Detection limit (M)	λem (nm)	Applicable pH range	Ref.
1	Cd coordination polymer	DMF	4.30×10^4	2.41×10^{-6}	502	5-7	[1]
2	Polymers based on di (naphthalen-2-yl)-1,2-diphenylethene	H_2O/THF (9/1)	4.70×10^4	1.81×10^{-6}	529	-	[2]
3	Zn-MOF	DMF	6.19×10^4	5.60×10^{-7}	434	-	[3]
4	Triazine-COF	THF	8.71×10^4	10.7 ppm	485	-	[4]
5	Nanoscopic organic cage	DCM	2.20×10^5	6.4 ppb	435	-	[5]
6	Gemini-iridium (III) complex	Water	3.22×10^4	1.20×10^{-7}	540	1-13	[6]
7	Ni(II)-compound	Water	6.80×10^4	1.62×10^{-6}	385	–	[7]
8	Tb coordination polymer	DMF	4.50×10^4	4.74×10^{-7}	416	-	[8]
9	Diphenylfumaronitriles	H_2O/THF (8/2)	5.60×10^4	1.80×10^{-10}	389	-	[9]
10	Iridium(III) complex	DCM	1.90×10^4	1.00×10^{-7}	466	-	[10]
11	Platinum(II) metallacycle-cored supramolecular	DCM	1.30×10^5	3.01×10^{-7}	506	-	[11]

12	Imidazole derivatives	H_2O/DMF (9/1)	1.30×10^4	3.55×10^{-6}	574	-	[12]
13	Thiophene aromatic amine derivatives	THF	-	5.70×10^{-6}	454	6.5-8.0	[13]
14	Sugar-based derivatives	Water	1.71×10^3	5.20×10^{-8}	537	-	[14]
15	Ni(II)-MOF	Water	1.30×10^5	2.60×10^{-7}	395	-	[15]
16	3-(Benzyloxy)-2-(4-(di-p-tolylamino)phenyl)-4H-chromen-4-one	Water	1.93×10^4	3.70×10^{-9}	525	4-11	[16]
17	[P(dimethylacrylamide-*co*-benzophenone acryl-amide-*co*-glycidyl methacrylate]	Water	7.75×10^4	5.60×10^{-7}	395		[17]
18	Iridium(III) complex	HEPES buffer /MeCN (9/1)	1.50×10^5	2.30×10^{-7}	500	7.3	[18]
19	9,14-diphenylpyreno [4,5-g]isoquinoline	MeCN	-	2.42×10^{-6}	447	-	[19]
20	7,10-bis(4-bromophenyl)-8,9-bis(4-(2-(2-(2-metho-xyethoxy)ethoxy)ethoxy)-phenyl)-fluoranthene	EtOH	5.60×10^5	2.6 ppb	480	-	[20]
21	Pyridoxamine-GSH-Copper nanoclusters	Water	7.80×10^4	2.74×10^{-8}	410,625	-	[21]
22	Fluorescein derivatives	EtOH	2.50×10^5	1.10×10^{-7}	517	-	[22]
Our job	1,3-Bis(benzo[d]thiazol-2-yl)benzene derivatives	H_2O/THF (9/1)	1.54×10^5	6.14×10^{-8} (29.1 ppb)	635	5-13	-

36. Supplementary material reference

[1] J. F. Zhang, J. J. Wu, G. D. Tang, J. Y. Feng, F. M. Luo, B. Xu and C. Zhang, *Sens. Actuators, B*, 2018, **272**, 166.

[2] Y. P. Zhuang, J. Y. Yao, Z. Y. Zhuang, C. J. Ni, H. M. Yao, D. L. Su, J. Zhou and Z. J. Zhao, *Dyes Pigm.*, 2020, **174**, 108041.

[3] S. H. Xing, Q. M. Bing, H. Qi, J. Y. Liu, T. Y. Bai, G. H. Li, Z. Shi, S. H. Feng and R. R. Xu, *ACS Appl. Mater. Interfaces*, 2017, **9**, 23828.

[4] Y. J. Li, Y. N. Han, M. H. Chen, Y. Q. Feng and B. Zhang, *RSC Adv.*, 2019, **9**, 30937.

[5] K. Acharyya and P. S. Mukherjee, *Chem. Commun.*, 2014, **50**, 15788.

[6] S. L. Yi, Z. Lu, Z. H. Xie and L. X. Hou, *Talanta*, 2020, **208**, 120372.

[7] J. X. Li, X. R. Zhuang, N. X. Zhang, L. Y. Zhao, Q. F. Yang and X. Zhang, *Inorg. Chim. Acta*, 2019, **497**, 119096.

[8] J. H. Cheng, Z. P. Liu, D. K. Wang, K. X. Chen, Y. J. You and X. H. Zhou, *Appl Organometal Chem.*, 2019, **33**, e5168.

[9] D. B. Wu, W. J. Gong, H. M. Yao, L. M. Huang, Z. H. Lin and Q. D. Ling, *Dyes Pigm.*, 2020, **172**, 107829.

[10] W. Y. Dong, Q. H. Ma, Z. H. Ma, Q. Duan, X. L. Lü, N. N. Qiu, T. Fei and Z. M. Su, *Dyes Pigm.*, 2020, **172**, 107799.

[11] Y. L. Hou, S. S. Li, Z. Y. Zhang, L. Chen and M. M. Zhang, *Polym. Chem.*, 2020, **11**, 254.

[12] S. S. Zhang, H. C. Zhu, J. Y. Huang, L. Kong, Y. P. Tian and J. X. Yang, *ChemistrySelect*, 2019, **4**, 7380.

[13] X. Lu, G. C. Zhang, D. D. Li, X. H. Tian, W. Ma, S. L. Li, Q. Zhang, H. P. Zhou, J. Y. Wu and Y. P, *Dyes Pigm.*, 2019, **170**, 107641.

[14] X. D. Yu, J. B. Guo, P. Peng, F. J. Shen, Y. J. Li, L. J. Geng and T. Wang, *Appl. Surf. Sci.*, 2019, **487**, 473.

[15] R. Goswami, N. Seal, S. R. Dash, A. Tyagi and S. Neogi, *ACS Appl. Mater. Interfaces*, 2019, **11**, 40134.

[16] Z. J. Luo, B. Liu, S. F. Si, Y. J. Lin, C. S. Luo, C. J. Pan, C. Zhao and L. Wang, *Dyes Pigm.*, 2017, **143**, 463.

[17] M. Gupta and H. Lee, *ACS Appl. Mater. Interfaces*, 2018, **10**, 41717.

[18] W. L. Che, G. F. Li, X. M. Liu, K. Z. Shao, D. X. Zhu, Z. M. Su and M. R. Bryce, *Chem. Commun.*, 2018, **54**, 1730.

[19] X. L. Yu, J. Q. Wan, S. Chen, M. Li, J. K. Gao, L. Yang, H. S. Wang, D. G. Chen, Z. Q. Pan and J.

B. Li, *Talanta*, 2017, **174**, 462.

[20] S. Kasthuri, S. Kumar, S. Raviteja, B. Ramakrishna, S. Maji, N. Veeraiah and N. Venkatramaiah, *Appl. Surf. Sci.*, 2019, **481**, 1018.

[21] R. Patel, S. Bothra, R. Kumar, G. Crisponi and S. K. Sahoo, *Biosens. Bioelectron.*, 2018, **102**, 196.

[22] Z.-H. Fu, Y. W. Wang and Y. Peng, *Chem. Commun.*, 2017, **53**, 10524.